Sérgio Ferreira Rodrigues

**Films based on biodegradable polymers
and graphene for biomedical applications**

Sérgio Ferreira Rodrigues

Films based on biodegradable polymers
and graphene for biomedical applications

outubro de 2018

Universidade do Minho
Escola de Engenharia

Sérgio Ferreira Rodrigues

Films based on biodegradable polymers
and graphene for biomedical applications

Dissertação de Mestrado
Ciclo de Estudos Integrados Conducentes ao
Grau de Mestre em Engenharia de Materiais

Trabalho efectuado sob a orientação de
Professora Doutora Maria da Conceição de Jesus Rego
Paiva
Professora Doutora Natália Maria Araújo Alves

outubro de 2018

DECLARAÇÃO

Nome: Sérgio Ferreira Rodrigues

Endereço eletrónico: sergio.f.rodrigues18@gmail.com   Telefone: 967717041

Cartão do Cidadão: 14848947

Título da dissertação: Films based on biodegradable polymers and graphene for biomedical applications

Orientadores:

Professora Doutora Maria da Conceição de Jesus Rego Paiva

Professora Doutora Natália Maria Araújo Alves

Ano de conclusão: 2018

Mestrado Integrado em Engenharia de Materiais

É AUTORIZADA A REPRODUÇÃO INTEGRAL DESTA DISSERTAÇÃO APENAS PARA EFEITOS DE INVESTIGAÇÃO, MEDIANTE DECLARAÇÃO ESCRITA DO INTERESSADO, QUE A TAL SE COMPROMETE.

Universidade do Minho, _____/_____/_____

Assinatura: _____

AGRADECIMENTOS

No momento da conclusão de 5 anos de universidade foram vários os momentos que vivi e, essencialmente, as pessoas que conheci. Não posso deixar de agradecer a todos esses que me têm vindo a acompanhar nesta jornada.

Em primeiro lugar, queria agradecer às minhas orientadoras, professoras Conceição Paiva4 e Natália Alves, por toda a orientação, apoio, confiança no meu trabalho e, especialmente, pela oportunidade de aprender e de crescer enquanto profissional. Obrigado por me terem transmitido conhecimentos importantes com este trabalho.

Em segundo lugar, ao Engenheiro Maurício e ao professor Paulo Lopes por toda disponibilidade em ajudar em todas as dúvidas e ensaios laboratoriais que foram realizados.

Agradecer a todas as pessoas que me acompanharam no laboratório que tornaram o ambiente muito agradável e sempre com boa disposição.

Quero também agradecer a todos os meus companheiros e amigos de curso pela amizade, apoio, paciência, e por terem vivido comigo todas as experiências que tornam a vida académica inesquecível.

E por fim, o mais importante, um especial agradecimento aos meus pais que me proporcionaram todos os meios para frequentar o curso e por todas as palavras de incentivo no decorrer de todos estes anos. Aos meus irmãos e à minha namorada um enorme obrigado por toda a ajuda, atenção prestada e palavras de encorajamento quando as coisas corriam menos bem.

UM ENORME OBRIGADO A TODOS!

RESUMO

Em várias aplicações biomédicas, uma das principais desvantagens dos polímeros biodegradáveis é seu baixo desempenho mecânico. A incorporação de cargas como grafite, derivados de grafeno, nanotubos de carbono e fulerenos em polímeros atraiu a atenção dos cientistas, devido às propriedades promissoras destes materiais compósitos na área biomédica. Neste trabalho, estudou-se a influência da incorporação de grafeno funcionalizado em matriz de poli (álcool vinílico) (PVA), com o objetivo de produzir PVA e seus filmes compósitos com propriedades melhoradas. Os filmes foram produzidos através da técnica de spray coating, visando sua aplicação no campo biomédico.

As suspensões aquosas de grafeno funcionalizado foram produzidas com sucesso através de exfoliação estabilizada em fase líquida, utilizando grafite como precursor. Uma incorporação máxima de 5% em peso de grafite exfoliada (EG) foi estimada como reforço.

As propriedades mecânicas e elétricas foram avaliadas por ensaios de tração uniaxial e medições de condutividade elétrica, respetivamente. A incorporação de EG levou a uma melhoria na resistência mecânica, assim como uma diminuição na resistividade elétrica também foi notada, apresentando valores próximos aos materiais semicondutores. A espectroscopia Raman revela a presença de grafite exfoliada. As propriedades térmicas foram avaliadas através da calorimetria diferencial de varrimento (DSC) e análise termogravimétrica (TGA), que apresentam uma diminuição na temperatura de transição vítrea, temperatura de fusão e temperatura de degradação com o aumento de grafite exfoliada. A morfologia dos filmes compósitos foi avaliada por microscopia eletrónica de varrimento (SEM). Imagens SEM revelam uma excelente homogeneidade através de toda a seção transversal dos filmes, o que confirma a melhoria nas propriedades mecânicas e elétricas. Relativamente aos ensaios de permeabilidade, os compósitos mostram um comportamento semelhante à matriz de PVA. Os resultados obtidos sugerem que os filmes de PVA reforçado com grafite exfoliada podem ter potencial aplicação em cicatrização de feridas e engenharia de tecidos cardíacos e ósseos.

ABSTRACT

In several biomedical applications, one of the major disadvantages of biodegradable polymers is their low mechanical performances. The incorporation of fillers, as graphite, graphene derivatives, carbon nanotubes and fullerenes in polymers attracted the attention of researchers because of the promising properties of this composite materials in biomedical field. In this work, was studied the influence of the incorporation of graphite and functionalized few-layer graphene in polyvinyl alcohol (PVA) matrix, with the purpose of producing PVA and their composites films with improved properties. The films were produced through spray coating technique, envisaging their application in the biomedical field.

Aqueous suspensions of functionalized few-layer graphene were successfully produced through stabilizer-assisted liquid phase exfoliation using pristine graphite as precursor. A maximum incorporation of 5 wt% exfoliated graphite (EG) has been estimated as reinforcement.

The mechanical and electrical conductivity was evaluated by uniaxial tensile tests and electrical conductivity measurements, respectively. The incorporation of EG led to films with an improvement in the mechanical strength, as well as a decrease in the electrical resistivity was also noticed, presenting values close to semiconductor materials. Raman spectroscopy reveals the presence of exfoliated graphite. The thermal properties were evaluated through differential scanning calorimetry (DSC) and thermogravimetric analysis (TGA), which presents a decrease in glass-transition temperature, melting temperature and degradation temperature with the addition of exfoliated graphite. The morphology of composite films was evaluated by scanning electron microscopy (SEM). SEM images reveals an excellent homogeneity through the entire cross-section of films, which testify the improvement in mechanical and electrical properties. Relatively to the permeability assays, the composites show a similar behaviour to the PVA matrix. The results obtained in this thesis suggest that PVA reinforced with exfoliated graphite films may have potential for wound healing and tissue engineering of cardiac and bone tissues.

LIST OF ABBREVIATIONS

B
BC - Bacterial Cellulose

C
CCG - Chemically converted graphene
CHI – Chitosan
CNT - Carbon nanotubes
CNWs - Cellulose nanowhiskers
CVD - Chemical vapor deposition

D
DMC - methacryloxyethyltrimethyl ammonium chloride
DSC - Differential Scanning Calorimetry

E
EG - Exfoliated Graphite

F
FGS - Functionalized graphene sheets
FLG - Few-layer graphene

G
GIC's - Graphite intercalation compounds
G – Graphene
GNP - Graphene Nanoplatelets
GO - Graphene oxide
GONS - Graphene oxide nanoparticles

L
LPE - Liquid Phase Exfoliation

N
NanoG – Nano Graphene

P
PANI - Polyaniline
PANI-NFs - Polyaniline nanofibers
PC - Polycarbonate
PE - Polyethylene
PEDOT:PSS - Poly(3,4-ethylenedioxythiophene) polystyrene sulfonate
PEI -mGO - Polyethylenimine- graphene oxide modified
PET - Polyethylene terephthalate
PVA-S - Sulfated Polyvinyl alcohol
PVC - Polyvinyl chloride
PVP - Polyvinylpyrrolidone
PY - Pyrene

R
rGO- reduced Graphene Oxide

S
SEM - Scanning Electron Microscopy
SiO$_2$ - Silicon Dioxide
SiC - Silicon Carbide
SRGO - Sulfonated graphene oxide

T
TGA - Thermogravimetric Analysis

U
UV-Vis - Ultraviolet Visible

W
WVT - Water Vapour Transmission

TABLE OF CONTENTS

LIST OF FIGURES

LIST OF TABLES

CHAPTER 1.

INTRODUCTION

1. INTRODUCTION

1.1. MOTIVATION

Due to recent advances in nanoscience's and nanotechnologies, a growing interest has been emerging in composites and nanocomposites for biomedical applications such as tissue engineering, biosensors and drug delivery systems [1]. Implants and medical devices are extremely used in the reposition or restoration of traumatized or degenerate tissues or organs. The materials used in these devices and implants must be biocompatible and/or biodegradable in order to avoid their rejection by the human body.

Among all synthetic biocompatible polymers, polyvinyl alcohol (PVA) is one of the most versatile, because its properties can be adjusted by chemical or physical modifications, allowing to improve its stability and its application in the release of drugs and in tissue regeneration. Thermal treatments and the production of composite materials are the most commonly used physical modifications to improve the performance of PVA in a wide range of applications [2,3].

Since 2004, when Geim and Novoselov found a way to isolate graphene [4], this material attracted the researcher's attention to its application in several areas, in particular the field of biomedical engineering. Graphene and its derivatives, including graphene oxide and reduced graphene oxide, have several characteristics that make them potential candidates for biomedical applications, like its low toxicity, biocompatibility, biofunctionality, exceptional mechanical properties, electrical conductivity and thermal stability [1,5].

In the present work it's intended to introduce graphene in the PVA matrix with the objective of producing PVA composite films. It is expected that these films will present several promising properties, which pure PVA would never present, essentially for various biomedical applications, namely in tissue engineering, biosensors and implant coatings.

1.1. Graphite

1.1.1. Structure

The name graphite was invented by Abraham Werner in 1789, it is a Greek word, *graphein*, which means "to write" [6]. In fact, graphite has been used since prehistoric times as a decorative pigment. In the 18th century, the chemist Scheele identified graphite as a carbon allotrope, until then graphite was considered a lead derivative due to its appearance [7].

The structure of graphite consists in a succession of layers parallel to the basal plane with carbon atoms with sp^2 hybridization attached in the form of hexagon, forming a continuous series of hexagons that can essentially be considered an infinite two dimensional molecule [7]. The ideal structure is represented in Figure 1. In this stable hexagonal structure, the interatomic distance is 1.42 Å and the distance between layers is 3.35 Å [6,7]. The stacking of basal planes can occur in two distinct ways: hexagonal or rhombohedral [8]. In the rhombohedral graphite the stacking occurs in the sequence -ABCABCABC-, however this crystalline system in the graphite is thermodynamically unstable and can be considered as a failure in the stacking of hexagonal graphite [9].
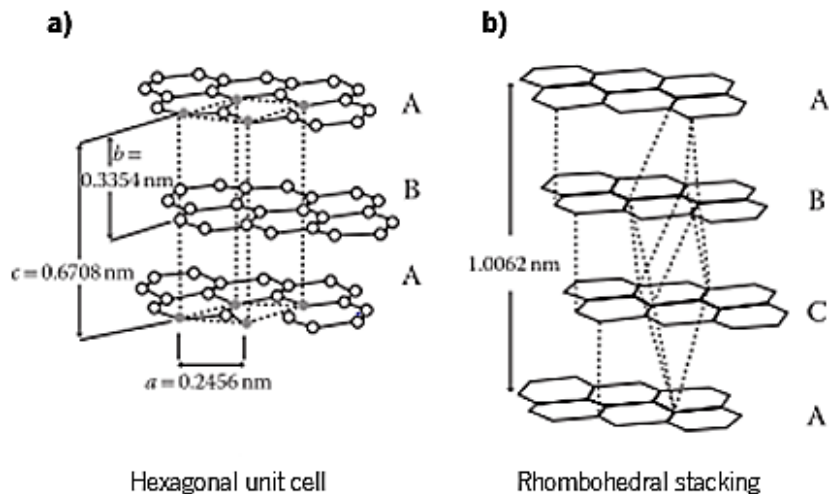
Figure 1: *Stacking of basal planes a) hexagonal and b) rhombohedral of graphene layers in graphite* [10]

In graphite structure, only three of the four valence electrons of carbon form regular covalent bonds (σ bonds) with adjacent carbon atoms. The fourth electron resonates between the valence structures. Stronger bonding forces exist within the planes of each layer, but the bonding energy between planes is only about two percent of the energy between atoms of the same plane. These weaker links between layers are more often explained as the result of van der Waals forces.

Chapter 1. Introduction

The differences between the electronic distribution and the forces within the planes and perpendicular to them result in the anisotropic properties of graphite especially with regard to electrical, thermal, and mechanical properties [7,11].

1.1.2. Properties

Graphite is an abundant material, with low cost of acquisition and interesting properties, especially when used as reinforcement in composite materials.

In terms of physical properties, the theoretical density of a graphite crystal is 2.26 g/cm^3, most graphite materials having a lower density due to the presence of imperfections in their structure, such as porosity. At atmospheric pressure, graphite has no melting point, but a sublimation point at a temperature of approximately 4000K. However, it is possible to obtain molten graphite inducing a pressure of 100 atm and a temperature of 4200K [7] into the system. Thus, among all elements, this is considered the most refractory material.

Unlike the physical properties (except density), the thermal properties are strongly affected by the size and the orientation of crystallites in the aggregates and also by other factors related to the processing conditions. As for the specific heat, graphite has values of 0.706 kJ/kg·K for a temperature of 298 K and a pressure of 1 atm, it is also reported that the increase in temperature causes a significant increase of specific heat [12].

Thermal conductivity of graphite is strongly influenced by the anisotropy of the material. Values reported for highly crystalline graphite, pressure annealed and pyrolytic graphite, relative to the basal plane, are 3000 W/m·K [11] and 4180 W/m·K at 298K [7]. For commercial pyrolytic graphite lower values are reported of 390 W/m·K, but it still remains a high value, and as a result graphite is considered a good thermal conductor when compared to other ceramics and metals. In relation to the perpendicular plane relative to the basal plane, graphite has very low thermal conductivity, making it an insulating material, having values of approximately 2 W/m·K and 6 W/m·K [7,11,13].

The coefficient of thermal expansion is also dependent of the direction and it shows values of 1×10^{-6} K^{-1} for the basal plane and 29×10^{-6} K^{-1} for the perpendicular, not increasing linearly with temperature [11].

In what concerns the electrical properties, graphite is classified as a semi-metal, which behaves as a conductor in the basal plane and as an insulator in the perpendicular plane. An

electrical conductivity of 2.26 × 10^4 Ω^{-1}·cm^{-1} and 5.9 Ω^{-1}·cm^{-1} are reported for the basal plane and perpendicular to the basal plane, respectively at 300K [14].

In the basal plane, Young's modulus of graphite is estimated at a value of 1 TPa, in this same direction the tensile strength is 130 GPa. In the perpendicular direction, graphite has an elastic modulus 30 times smaller than in the basal plane direction [7].

Graphite is considerably inert in chemical terms, being resistant to most acid, alkaline and corrosive gases [7]. However, in both pure and synthetic graphite the presence of impurities is usual, and they will cause an increase in chemical reactivity, reducing the resistance to the chemical environments referred. The porosity is another factor that affects the reactivity of graphite, because with the increase of porosity the surface area will increase too [10]. The major exception to the excellent chemical resistance of graphite is its low resistance to the elements of Column VI of the periodic table, particularly to oxygen and oxygen compounds [7].

Concerning the production of nanocomposites, new methodologies to obtain graphite structures with few layers of graphene and nanometric thickness are under investigated, leading to the production of exfoliated graphite (EG).

Natural graphite is easily intercalated, due to the weakness of van der Waals bonds, by different chemical species, or intercalation agents, which can be atoms, molecules, metallic compounds and salts [11]. The intercalation of several chemical species originates graphite intercalation compounds (GIC), which allow the exfoliation of graphite. The most conventional method to promote the exfoliation of GIC's is their submission to a thermal shock, involving a large expansion of the interlayer (up to hundreds of times) along the stacking axis [14]. Due to the vaporizing tendency, the interlayer gas pockets are formed which can explode. The expansion of the gas pockets is improved by the shearing of graphite layers. If the gas pockets do not burst and the heating is not excessive, the exfoliation can be reversible when the temperature is dropped. However, an excessive heating causes irreversible exfoliation [15,16].

Exfoliated graphite is a material with low density and high resistance to temperature, so it may be used as an reinforcing material; it is resistant to fire, acting as a self-extinguishing agent; thermal insulation; electrical conductor that is used for conductive composite resins; high corrosion resistance [17]. It can also be used in electrodes, packaging, membranes for gas permeability and lubricants [18].

1.2. Graphene

1.2.1. Structure

The interest in graphene has grown exponentially over the past few years due to its excellent properties (mechanical, optical, electrical, thermal) and a wide range of possible applications in various scientific fields [19].

Graphene is the name given to a material consisting of one planar sheet in the constitution of graphite, which is composed by carbon atoms with sp^2 bonds, forming a hexagonal two-dimensional (2D) honeycomb network, where the length of the bond between the two carbon atoms is 0.142 nm and bond strength is 524 kJ / mol [7, 9]. The referred structure is shown in Figure 2.
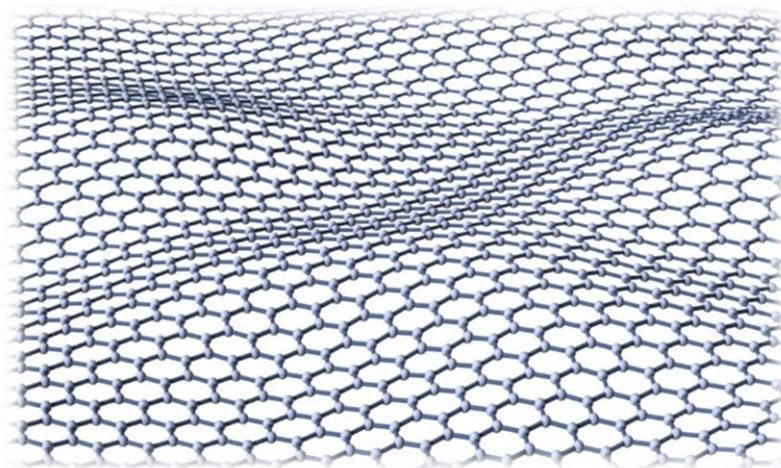
Figure 2: *Structure of graphene* [21]

In the structure of graphene, sp^2 hybridization is the result of the combination of a 2s orbital with two 2p orbitals and this is the mechanism of generation of three identical hybrid sp^2 orbitals [22]. Each carbon atom with sp^2 hybridization combines with other identical carbon atoms to form a network with hexagonal structures, as described above for the constitution of the single layer that stacks to form the structure of graphite [7,23].

The fourth orbital in graphene, that may be described as the delocalized, non-hybridized orbital containing the p electron, is oriented perpendicular to the basal plane. This orbital is the remaining 2p orbital on each carbon and it overlaps with its three neighbouring carbons to form a band of filled π orbitals, known as the valence band, and a band of empty π* orbitals, called the conduction band [24,25]. These highly-mobile electrons (π electrons) are located above and below the graphene sheet and they are primarily responsible for the electrical and optical properties in these systems. Sigma bonds are in charge of mechanical properties [24].

In what concerns the band structure, π bands touch at six points, that are called Dirac or charge neutrality points. Symmetry allows these six points to be reduced to two inequivalent points, K and K′ (Figure 3a). Each unit lattice of graphene has two carbon atoms that cause two equal conical intersection points (K and K′) in each Brillouin zone, and the energy at the intersection point is linearly related to the wave vector (Figure 3b). Thus, the effective mass of electrons and holes in graphene is zero, and all electrons and holes are called Dirac fermions. At Dirac point, the energy near it is zero, and the bandgap of graphene is zero [26,27]. If we limit ourselves to low energies, which are the most relevant in electron transport, the bands have a linear dispersion. The fact that these bands touch at E_{Dirac} indicates that graphene has no energy at band gap, and it is therefore usually described as a zero-gap semiconductor [28].
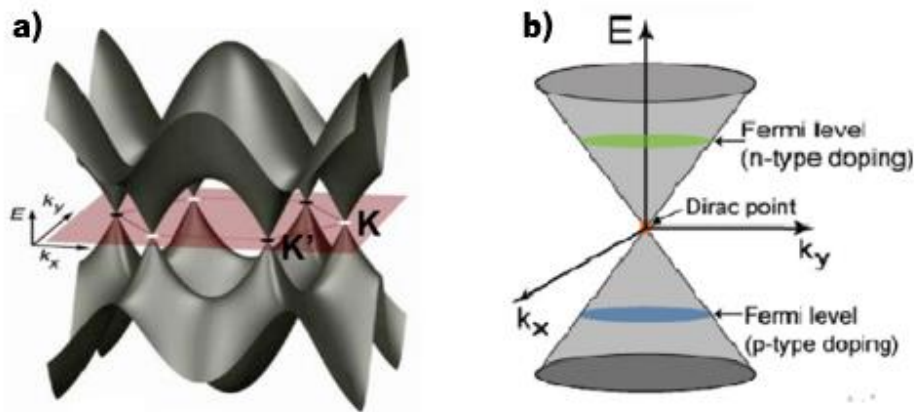
Figure 3: a) The 3D band structure of graphene. b) Approximation of the low energy band structure as two cones touching at the Dirac point [28]

1.2.2. Properties

Because of its structure, graphene presents excellent mechanical, electrical and thermal properties. In terms of thermal properties, Balandin, et al. reported that a suspended graphene sheet produced by mechanical exfoliation could exhibit extremely high thermal conductivity values ranging from 4840 to 5300 W/mK [29]. However, W. Cai, A. Moore, Y. Zhu et al. experimental results on CVD grown suspended graphene indicate lower values 2500 W/mK [30]. The variance in conductivity values may be due to the different production techniques.

Another of graphene's stand-out properties is its inherent strength. For an individual graphene sheet the breaking strength is 200 times larger than that of steel, with a Young's modulus of 1 TPa and a tensile strength of 130 GPa [31]. The high elastic properties make graphene able

to retain its initial size after strain. These measurements stablish that graphene is one of the strongest materials ever measured.

At low temperatures and high magnetic fields, the exceptional mobility of graphene allows for the observation of the quantum hall effect for both electrons and holes. Due to its unique band structure, the graphene quantum hall effect exhibits a subtle difference from the conventional quantum Hall effect and the anomalous half-integer quantum Hall effect [32]. Electronic mobility values of 15000 $cm^2 \cdot V^{-1} \cdot s^{-1}$ [32] and 200000 $cm^2 \cdot V^{-1} \cdot s^{-1}$ [33] were reported which may mean ballistic transport.

Graphene is a material with almost total transparency and their ability to absorb a rather large 2.3% of white light is also a unique and interesting property, especially considering that it is only 1 atom thick. This is due to its electronic properties; the electrons acting like massless charge carriers with very high mobility [34].

Other intrinsic properties of graphene are their surface area 2630 m^2g^{-1}, which is much greater than that of graphite 10 m^2g^{-1} and even that of carbon nanotubes 1315 m^2g^{-1} [35]; impermeability to gases and their considerable chemical inertia. Another interesting property of graphene is that, although it is relatively inert, it can be chemically functionalized using the adequate chemistry [4].

1.2.3. Production techniques

From its discovery, along with scientific development, various methods for producing graphene have been developed and are continually improved. Depending on the quality of the desired product and the intended application, one or more methods may be used.

There are several techniques reported for the production of graphene, such as mechanical exfoliation of graphite, chemical vapor deposition, plasma enhanced chemical vapor deposition, thermal decomposition on silicon carbide (SiC) substrates and reduction of graphene oxide (GO).

i.   Mechanical exfoliation

Mechanical exfoliation was the first technique employed to prepare graphene. This was successfully done by Novoselov *et al.* to prepare graphene from monocrystalline graphitic film [36]. This method is a laborious procedure where the probability of finding individual graphene sheets of good quality is often low [37].

ii.   <u>Chemical vapor deposition (CVD)</u>

Chemical vapor deposition growth has been reported as the most promising technique for large-scale production of mono- or few-layer graphene film. This process consists in the decomposition of a carbon gas precursor, such as a mixture of methane and hydrogen [20], into carbon atoms, which deposits and dissolves at the surface of metal foils such as copper and nickel [8], under inert atmosphere and high temperature. Then, the metal substrate is etched to detach the graphene layers so that they can be transferred to a new substrate. The quality of graphene layers can be optimized by controlling the reaction parameters, substrate and the type of carbon precursor [36].

Somani *et al.* reported the first successful production of few layer graphene films using CVD by using nickel as foils and camphor as carbon source [38].

The major drawback of the chemical vapor deposition technique is that it is an expensive process owing to the large energy consumption and the necessity of removal of the underlying metal layer [4].

iii.   <u>Thermal decomposition on SiC substrates</u>

The technique of thermal decomposition on SiC substrates uses silicon carbide, in the form of wafers, to produce graphitic layers. Silicon carbine is the most common material used in high-power electronics and because of that, this technique is an attractive approach for the field of electronics. The production of graphene by this technique consists in exposing SiC wafers to ultra-high vacuum and heating to 1250°C to promote the sublimation of Si atoms, leaving a graphitized surface [4,39].

The major drawbacks of thermal decomposition on SiC are the high cost of SiC wafers and the high temperatures involved [40,41].

iv.   <u>Chemical reduction of graphene oxide</u>

Graphene can be produced from graphene oxide by inducing its reduction, and that can be carried out through various methods. Synthesis of GO was developed several decades ago by Brodie [42], Staudenmeier [43] and Hummers *et al.* [44] and these methods remain in use today with only minor modification. All these methods involve the oxidation of graphite to various levels with different solvents, followed by sonification. Brodie and Staudenmaier's methods the oxidation

process generates ClO_2 gas that is a highly toxic gas. Hummers method is the most used in current research because it has shorter reaction time and doesn't produce toxic gases, but it has one drawback that is a potential contamination by excess permanganate ions, which should be removed by treatment with H_2O_2 [37].

The oxidation process of graphite is typically carried out by combining graphite powder with sulfuric acid (H_2SO_4), nitric acid (HNO_3), potassium permanganate ($KMnO_4$) and sodium nitrate ($NaNO_3$) [26]. The introduction of oxygen functional groups results in an increase in the spacing between the graphite layers, making it possible to exfoliate into separate GO layers. Graphene can be produced from reduction of GO as well by using chemical or thermal reduction. Chemical reduction is done with hydrazine, $NaBH_4$, hydroquinone on vigorous stirring, however this technique results in a formation of strong defects and toxic waste which is dangerous to the environment. Thermal reduction is performed by a heat treatment and also induce defects on graphene structure [34,36]. Thus, environment-friendly and highly effective reducing agents are investigated to substitute the conventional methods to reduce GO [36]. Environment-friendly chemical reducing agents, such as vitamin C [45], aluminium powder [46] and reducing sugar [47] have been used to synthesize reduced GO. Wang *et al.* [48] showed that GO can be reduced by making use of the reducing capability and the aromatic rings of tea polyphenol that exists in green tea solution. The characterizations of the reduced graphene sheets confirmed the efficient removal of the oxygen-containing groups in GO. Their approach demonstrates that several advantages for large scale production of reduced graphene sheets, such as environmentally friendly reduction process, low cost and simple reduction procedure, no hazardous waste was produced.

v.   Stabilizer-assisted liquid phase exfoliation

The process of stabilizer-assisted liquid phase exfoliation consists in a direct exfoliation of graphite to graphene without production of graphene oxide. Most liquid phase methods involve the oxidation of graphite and then exfoliation is performed to form graphene oxide suspensions. GO is an electrically insulating material and so, in order to recover part of its conductivity, it needs to undergo a reduction process. This is normally achieved through chemical treatment with reducing agents or by heat treatment. A disadvantage associated to these methods is the formation of structural defects during the oxidation process, which will degrade the electronic and mechanical

properties of graphene [49]. In Figure 4 FLG production schemes are shown, with and without addition of stabilizers or surfactants. In the latter case the solvent used is strongly adsorbed at the graphene surface.
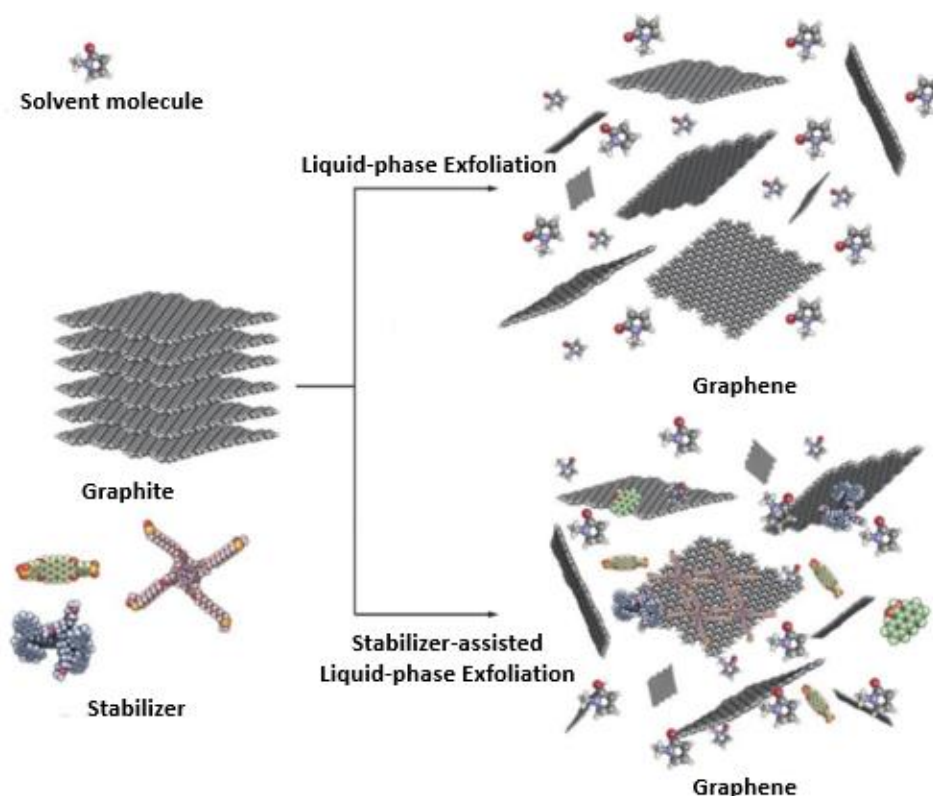
Figure 4: Scheme of production of functionalized few layer graphene, adapted from [50]

The use of solvents in the above-mentioned process plays a crucial role in exfoliation, since the energy required to exfoliate the graphite must be balanced by the solvent-graphene interaction [51]. Water and organic solvents are the most commonly used solvents. Due to its non-toxicity, water opens an excellent prospect for the formation of biocompatible graphene-based materials for biomedical applications. However, the exfoliation of graphene in water, a polar solvent, is limited by the hydrophobic nature of layers [50,52]. This problem can be solved by using stabilizers, such as polymers, surfactants, and amphiphilic aromatic compounds that will prevent the restacking of graphene sheets [49]. The most promising stabilizers to produce large quantities of graphene are polycyclic aromatic hydrocarbons such as pyrene derivatives. Adsorption of these compounds onto graphene surface occurs through π-π interactions between the planar surfaces of stabilizer and graphene [53,54]. To produce large quantities of graphene, a small concentration of pyrene is normally used, in contrast with the required concentrations when surfactants or polymers are used. The excess of stabilizer will affect the mechanical and electrical properties, as reported by Parviz

et al. [52]. Fundamentally, stabilizer-assisted liquid phase exfoliation consists in a preparation of a stable solution of an adequate surfactant, then add graphite powder to it and submit to ultrasounds. Finally, centrifugation of the suspension to remove graphite particles that did not exfoliate, and collection of the supernatant, containing the stabilized FLG.

Figure 5 represents various techniques for mass production of graphene and some applications that use graphene produced by each technique. There is also a relationship between the quality of the graphene produced as a function of the cost of production.
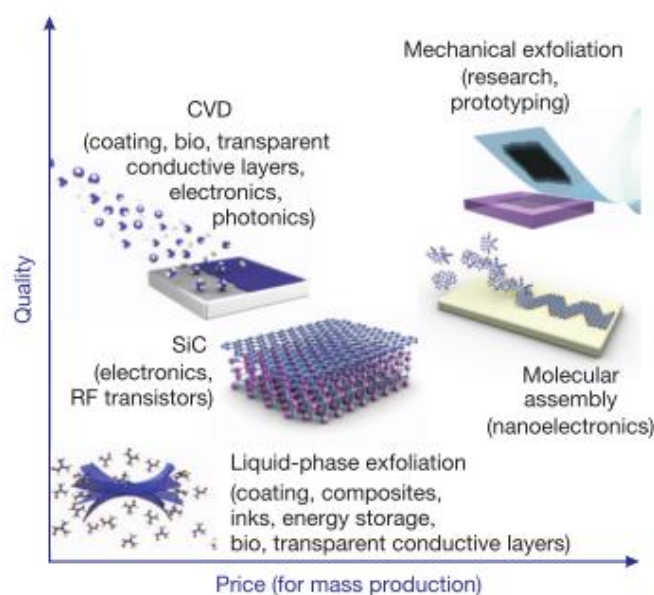
Figure 5: Quality of graphene vs price of production for several methods of mass production

1.2.4. Functionalization of graphene

The bottleneck for the application of graphene is its production at high yield and high quality, forming sheets with large surface area that may easily disperse in organic and inorganic solvents. The graphene sheets tend to stack and to form stable agglomerates through π-π interactions and van der Waals interactions if graphene layers are not well separated and stabilized [27,55,56].

In order to achieve a better performance or interfacial adhesion, it may be necessary to functionalize graphene. Graphene has a hydrophobic behaviour so, it is necessary to chemically modify its surface to produce stable aqueous suspensions [57]. The surface modification can be performed through covalent or non-covalent functionalization methods [58]. Covalent functionalization is usually performed by the oxidation of graphite and the formation of graphene

oxide (GO). This type of graphene is frequently used to form composites with strong interactions between graphene and matrix [59]. However, the original structure of graphene is strongly destroyed, leading to a decrease in electrical conductivity and mechanical properties. Non-covalent functionalization involves physical adsorption of specific molecules at the graphene surface through π-π interactions, electrostatic interactions, hydrogen bonds, coordination bonding and van der Waals forces [55,60]. This method of modification preserves the natural structure of graphene, preserving the sp^2 carbon hexagonal lattice, however, the interactions between the specific molecules and graphene surface are relatively weak, therefore is not suitable for some applications where strong interactions or interfaces are required [61].

Concerning non-covalent functionalization there are various methods that may be applied to the production and stabilization of graphene in liquids. Methods based on liquid phase exfoliation (LPE) are used for the exfoliation of graphite or expanded graphite and through these processes it's possible to obtain few layer graphene (FLG), defined as a type of graphite with a small number of layers, typically smaller than 7. In this work, the functionalization of graphene was performed directly from graphite, following a method known as stabilizer-assisted liquid phase exfoliation, a non–covalent approach.

1.3. Polyvinyl alcohol
1.3.1. Synthesis and properties

In 1924, Baum et al. [50] prepared polyvinyl alcohol (PVA) from vinyl acetate and since the then use of this material has attracted great attention, and extended to a large level production, finding industrial and biomedical applications, or common applications, due to its unique properties such as water solubility, biodegradability, excellent biocompatibility, low toxicity, film orientation characteristics, and adhesive properties [62–64].

Normally, the production of polyvinyl alcohol occurs in two stages due to the unstable form of vinyl alcohol as monomeric units, the first stage is the free-radical polymerization of vinyl acetate in an alcoholic solution and the second is the partial or full hydrolysis of polyvinyl acetate [65]. In Figure 6 it's possible to analyse the stages of polyvinyl alcohol preparation. Vinyl acetate can be easily polymerised in bulk, solution, emulsion and suspension. The polymerization starts when the radical at the tertiary carbon atom or at the acetate group is formed. Since polyvinyl acetate is used in an emulsion form, the emulsion polymerisation is usually used. Equal quantities of vinyl acetate

and water are stirred together in the presence of a suitable colloid-emulsifier system, such as sodium lauryl sulphate, and a water-soluble initiator such as potassium persulphate [66]. Then polyvinyl alcohol is produced by alcoholysis of a polyvinyl ester such as polyvinyl acetate. Sometimes the term hydrolysis is incorrectly used to describe this process. Methanol or ethanol can be either used to effect alcoholysis but the first one is preferred because of its miscibility with polyvinyl acetate at room temperature. Either acid or base catalysis can be employed, but only alkaline catalysts such as sodium hydroxide or sodium methoxide is able to accelerate alcoholysis [67]. Polyvinyl alcohol is available in several grades which diverge in molecular weight and in the residual acetate content, because alcoholysis will cause scission of branched polymers at the points where branching has proceeded via the acetate group [66].
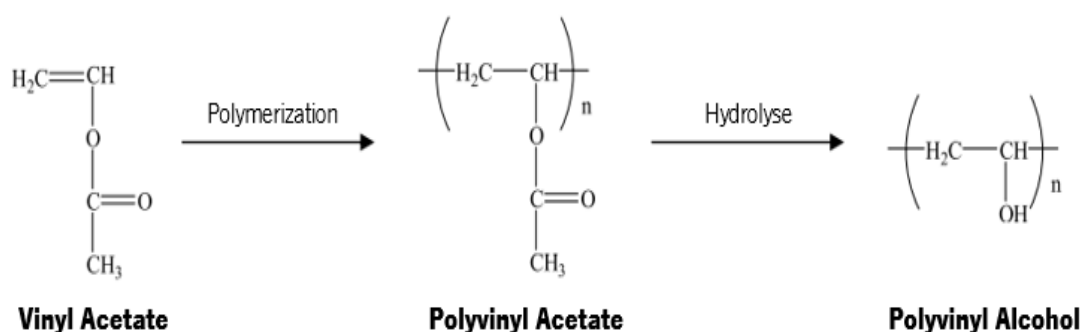
Figure 6: *Chemical reactions for production of polyvinyl alcohol - polymerization of vinyl acetate and hydrolysis of polyvinyl acetate to polyvinyl alcohol, adapted from* [66]

By controlling the hydrolysis process, different grades of polyvinyl alcohol with different hydrolysis degree can be prepared, which will affect its properties such as solubility, crystallinity, and chemical properties [68]. Polyvinyl alcohol with low hydrolysis degree shows higher solubility in water at low temperature as compared with high hydrolysis degree. Actually, residual acetate groups (hydrophobic in nature) weaken the intra and intermolecular hydrogen bonds of adjoining −OH groups and for polyvinyl alcohol with high degree of hydrolysis, temperature must be raised well above 70°C to dissolve in water. In 2000, Hassan and Peppas reported the influence of temperature in the hydrolyses degree of PVA with an average molecular weight M_n=77000 [65]. Figure 7 shows the solubility of a polyvinyl alcohol sample as a function of the hydrolysis degree at dissolution temperatures of 20°C and 40°C. It reveals that the increase of temperature will improve the solubility of polyvinyl alcohol in water for high values of hydrolysis degree [69].
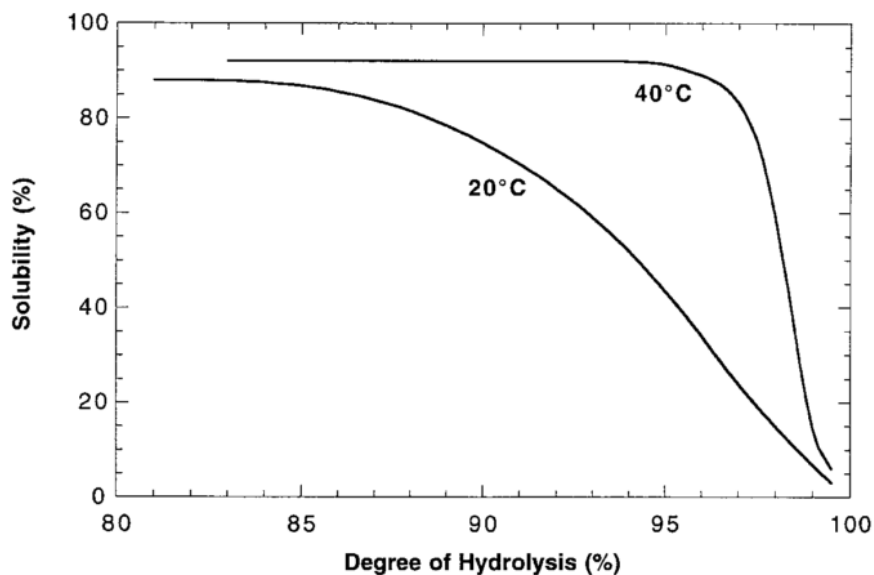
Figure 7: Influence of temperature in solubility and hydrolyses degree of PVA

1.3.2. Biodegradation

The global consumption of PVA is over one million tons per year and tends to increase at an overall rate of 3.5% annually. PVA, one of the most used vinyl polymers soluble in water, has been largely used in the textile and paper industries, which generate considerable amounts of PVA containing wastewaters that will contaminate the environment, as biodegradation of PVA usually proceeds very slowly [70].

Since 1936, when it was observed the biodegradation of PVA by an action of phytopathogenic fungus, *Fusarium lini*, studies were carried to investigate other bacteria to degrade PVA, such as *Pseudomonas* [71], *Bacillus magaterium* [72], *Flavobacterium*, *Acinetiobactor* [73], *Alcaligenes*, *Xanthamonas* [73,74] and *Phanerochaete chrysosporiu*.

The initial biodegradation step process involves the enzymatic oxidation of the secondary hydroxyl groups in PVA to ketone groups, which are subsequently hydrolysed to cleavage the polymer chain [75]. One of the most studied bacteria is *Pseudomonas* and its enzymes: SAO (*secondary alcohol oxidase*) PVDH (*PVA oxidase*) and BDH (*β-diketone hydrolase*). SAO is an extracellular enzyme that is purified from the culture supernatant of a *Pseudomonas* strain. This enzyme is responsible for the drop in PVA viscosity and for the oxidation step of PVA degradation, which is based on O_2 consumption and H_2O_2 production during the reaction, leading to the formation of β-hydroxyketone groups. The resulting β-diketone groups undergo hydrolytic cleavage by a specific enzyme, named by *β-diketone hydrolase*, produced and excreted in the culture

supernatant of *Pseudomonas*. The hydrolytic reaction does not require oxygen or other electron acceptors and promotes a fast drop in the viscosity of SAO-oxidized PVA solutions. These reactions result in a formation of shorter chains with butanone and carboxylic acid groups [71]. Two biodegradation pathways of PVA are represented in Figure 8, Figure 8a) is mediated by *secondary alcohol oxidase* (SAO) and *β-diketone hydrolase* (BDH), which is explained above, and in Figure 8b) is mediated by a specific *PVA-oxidase* and *β-diketone hydrolase* (BDH), which is similar to the previous process.
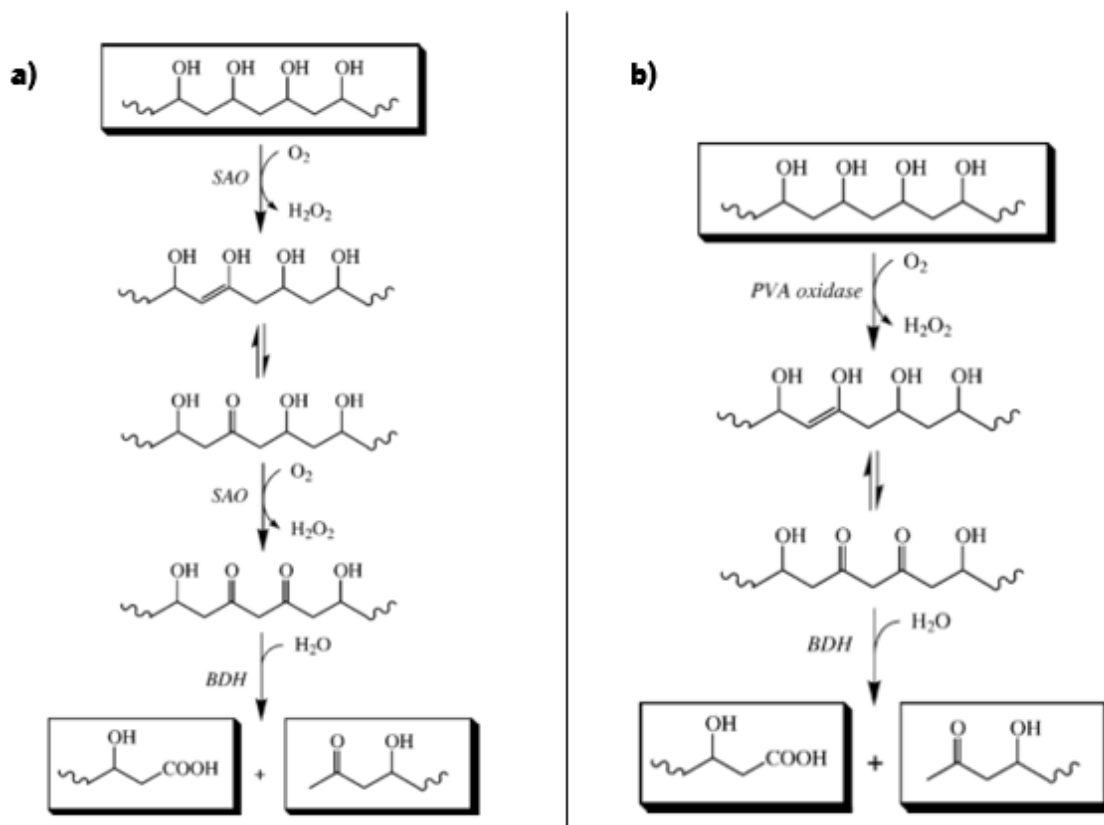
Figure 8: *Scheme of biodegradation pathways of PVA, mediated by a) secondary alcohol oxidase (SAO) and β-diketone hydrolase (BDH) and b) PVA-oxidase and β-diketone hydrolase (BDH)* [71]

Several authors have investigated the influence of the polymerization degree and hydrolysis degree on the biodegradation process of PVA. For example, Lee and Kim reported the polymerization degree effect on the biodegradation [75]. Samples of PVA-05, PVA-17 and PVA-24 with nearly the same hydrolysis degree of 88% were prepared. Figure 9 presents the results of PVA samples by *Cardiobacterium* SB68+SB69, a symbiotic pair. Th study concluded that the mineralization rate was nearly independent of the polymerization degree. It was also observed that the degradation of PVA with low molecular weight was poorly affected by the degree of polymerization.
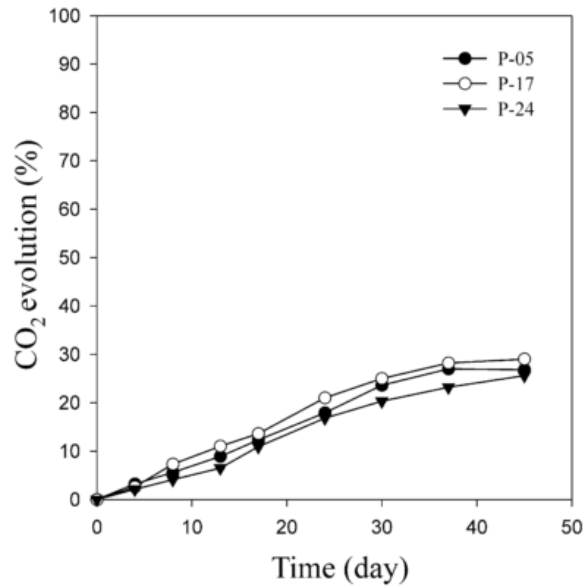
Figure 9: *Biodegradation test results of PVA-05, PVA-17 and PVA- 24 at 0.025% using the bacterial symbionts, SB68+SB69* [75]

In another study, E. Chiellini *et al.* [76] reported the influence of PVA with different hydrolysis degree, 72, 88 and 98%, on the biodegradation behaviour. Figure 10 shows the results obtained by a respirometric test in soil, where are shows the significant differences in the rate of biodegradation for the different samples. With these results it's possible to conclude that high values of hydrolysis degree results in low values of biodegradation.
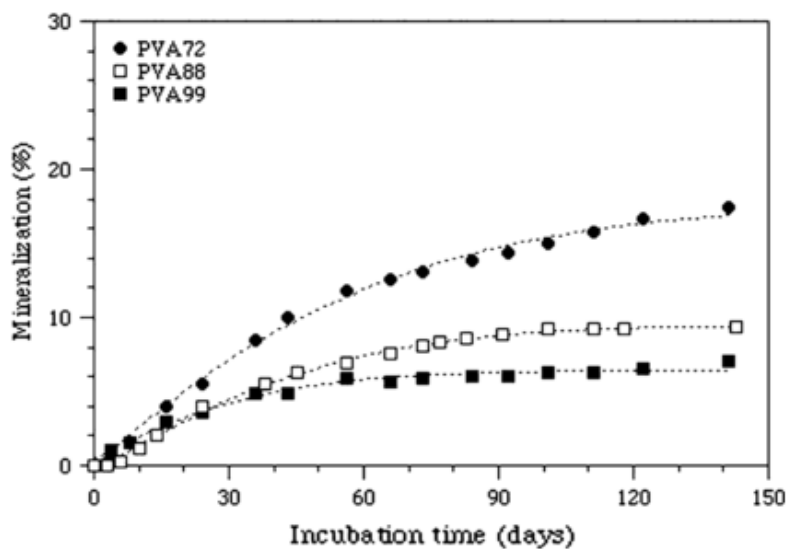
Figure 10: *Influence of hydrolysis degree on biodegradation behaviour of PVA 72, 88 and 98% samples in soil* [76]

1.3.3. Physical and chemical properties

The chemical and physical properties of PVA can vary based on the molecular weight and percentage of hydrolysis for the grade of PVA [77]. PVA itself has substantial tensile strength, flexibility, hardness and gas barrier properties. Its oxygen-barrier properties are superior to those of any known polymers; however, PVA must be protected from moisture, which greatly increases its gas permeability [78].

The water solubility and physical properties of PVA, including its film form, are highly affected by the degree of hydrolysis, molecular weight and crystal precipitation [79]. PVA is partially crystalline upon formation and is characterized by distinct properties such as chemical resistance, water solubility and biodegradability. PVA is biocompatible and non-cytotoxic [80,81], which explains the development of PVA membranes for biomedical applications such as skin tissue and bone repairing [82]. Biocompatibility studies were also addressed for PVA mixed with other materials. For instance, hydroxyapatite (HA), the main mineral component of bone, was combined with Gelatin and PVA by emulsification .[83]. This composite material was investigated *in vivo* by implanting it subcutaneously in the dorsal region of rats for 12 weeks. The results indicated that the HA/PVA/Gel is biocompatible and may serve as a cartilage scaffold for tissue engineering applications [83].

Because of their high capacity to absorb water, good oxygen permeability, optical transparency and low protein adsorption, PVA hydrogels have been used to make soft contact lenses [66]. High mechanical strength, rubber-like elasticity and low adhesion to surrounding tissue also make PVA hydrogels as potential candidates as scaffolds for different tissues, such as cartilage and invertebrate discs nuclei [66,84].

PVA's are very common polymers, widely used as surface materials in a huge range of fields as films and glues [85] due to their exceptional chemical and physical properties, biocompatibility, stability to temperature variation, and non-toxicity [86,87].

In the food industry, PVA's oral toxicity was reviewed by DeMerlis and Schoneker [77] concluding that PVA is an orally safe product to use. The LD_{50} reported was between 15 and 20 g/kg, indicating a low acute oral toxicity.

PVA also has a melting point of 230°C and 180–190°C for the fully hydrolysed and partially hydrolysed grades, respectively. Its thermal degradation usually starts at about 150°C or above, depending upon the PVA grade.

1.4. Films based on polyvinyl alcohol and graphene

Spray coating is a widely used technique for the production of films and coatings. This method is simple, quick, easy to handle and a low-cost process. The spray coating technique consists on the deposition of a suspension on a preheated substrate, so the solvent is evaporated and only the polymer and suspended particles remain deposited [88,89]. The film production technique by spray coating is schematically illustrated in Figure 11.
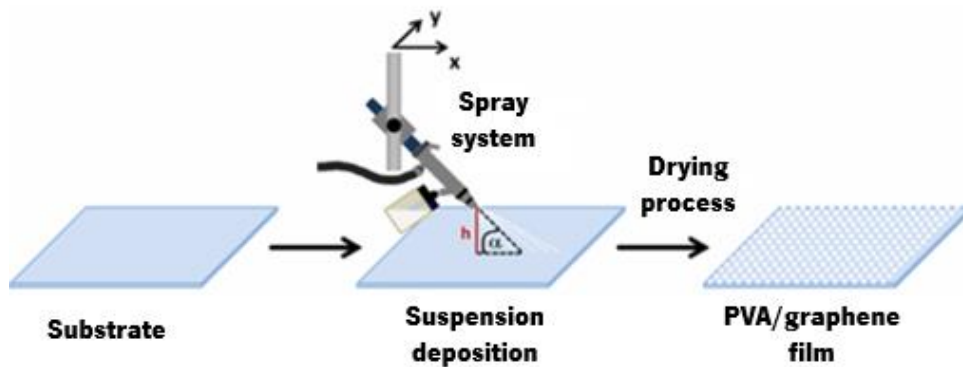
Figure 11: Scheme of manufacturing process of PVA/graphene films by spray coating, adapted from [90]

Spray coating is a high-throughput process that allows the deposition over a large surface area, ensuring optimal coatings on a variety of surfaces with different morphologies. In addition, this technique allows the access to a wide range of fluids with different rheology, being able to adjust the system to deposit any type of solution and obtain the desired properties of films. In this process the amount of waste produced is greatly reduced [91].

The production of graphene/graphene derivatives polymer composites has been a field of intense research. A detailed literature research was carried out to identify types of reinforcements combined with PVA matrices, as well as alternative polymer matrices that have been combined with graphene and its derivatives, for the production of films. The manufacturing processes used were identified as well as the applications intended. The results of this literature overview are compiled in Table 1.

Table 1: Composite materials with PVA matrix or reinforced by graphene and their derivates, produced by various techniques

Matrix	Reinforcement	% Reinforcement	Process	Mechanical P. Tensile Strength (MPa)	Electric P. Conductivity (S/m)	Application/ Study	Shape	Ref.
PVA	BC	12–27 wt.%	Casting-Drying	3.9	-	Artificial cornea	Film	[92]
PVA	CNWs	3 wt.%	Freezing–Thawing	1.1	-	Skin wound	Hydrogel	[93]
PVA	PVP	-	Freezing–Thawing	2.8	-	Cartilage tissue	Hydrogel	[94]
PVA	PU	-	-	39.87	-	Cartilage tissue	Hydrogel	[95]
PVA	GO	30 wt.%	Solution Casting	280	1×10^{-8}	Study of structure and properties	Film	[96]
PVA	RGO	30 wt.%	Solution Casting	65,7	1×10^{-3}	Study of structure and properties	Film	[96]
PVA	SRGO	30 wt.%	Solution Casting	235	1×10^{-4}	Study of structure and properties	Film	[96]
PVA	GO	0.7 wt.%	Solution Casting	87.6	-	Molecular-Level Dispersion of Graphene into PVA	Film	[97]
PVA	GO	1 wt.% GO4 (2g graphite e 8g KMnO$_4$)	Solution Casting	55	-	Effect of oxidation degree of GO	Film	[98]
PVA	PEI-mGO	3 wt.%	Solution Casting	122.6	-	Hydrogen gas barrier	Film	[99]
PVA	GO	4 ml de GO in solution	Solution Casting	-	0.073	Supercapacitor Applications	Film	[100]

Matrix	Reinforcement	% Reinforcement	Process	Mechanical P. Tensile Strength (MPa)	Electric P. Conductivity (S/m)	Application/ Study	Shape	Ref.
PVA	rGO	4 ml de GO In solution	Solution Casting	-	0.625	Supercapacitor Applications	Film	[100]
PVA	CNT	53 wt.%	Spray Winding	1000	7.47×10^4	Effect of different sprayed solution concentration	Film	[101]
PVA	CNT	56.8 wt.%	In Situ	3160	1.32×10^5	Study of the process	Film	[102]
PVA-S	NanoG	1.5 wt%	Solution Casting	28	5.4×10^{-5}	Morphology and Properties of PVA-S/NanoG	Film	[103]
PET	G	1.2 vol.%	Melt Compounding	-	7.4×10^{-2}	EMI Shielding	Samples	[104]
PET	Graphite	7.1 vol.%	Melt Compounding	-	2.45×10^{-4}	EMI Shielding	Samples	[104]
PVC	G	2 vol.%	Drop Casting	55	1×10^{-3}	-	Film	[105]
PANI	Graphite	1.5 wt.%	In Situ	-	3.33×10^3	Facile synthesis of PANI/Graphite	-	[106]
PANI-NFs	CCG	44 wt.%	In Situ	-	5.5×10^2	Supercapacitors devices	Film	[107]
PC	FGS	2 wt.%	Melt Compounding	-	1×10^{-9}	Gas Permeability	Bar, Disk and film	[108]
PC	Graphite	12 wt.%	Melt Compounding	-	6.6×10^{-11}	Gas Permeability	Bar, Disk and film	[108]

Matrix	Reinforcement	% Reinforcement	Process	Mechanical P. Tensile Strength (MPa)	Electric P. Conductivity (S/m)	Application/ Study	Shape	Ref.
PEDOT:PSS	GNP	20 wt.%	Spray coating	45	60	Conductive Synthetic Textiles	Fibers	[109]
PEDOT:PSS	G	0.02 wt.%	Substrate Vibration-Assisted Spray Coating	-	7.2×10^4	Transport Layer and Transparent Conductive Electrode	Film	[110]
SiO$_2$	GO	3.9 wt.%	Spin Coating	-	8×10^{-2}	Transparent Conductors	Film	[111]
PMMA	EG	5 wt.%	Solution Blending	-	1×10^{-4}	Study of E. Conductivity and Dielectric Properties	Film	[112]
PMMA	Graphite	5 wt.%	Solution Blending	-	1×10^{-5}	Study of E. Conductivity and Dielectric Properties	Film	[112]
CHI	GO	18 wt.%	Solution Casting	43.9	-	-	Film	[113]

According to the results reported in Table 1, it is observed that PVA and graphene derivatives have been the object of intense study for several years. Studies carried out on these materials are mostly focused on the investigation of new processes of film production and the study of their electrical properties. The applications of graphene reinforced composites are largely in electrical devices because graphene is a material with excellent electrical properties and when impregnated in polymer matrices increases the electrical conductivity of the formed composites, making them promising to obtain an excellent performance of devices.

PVA and PVA matrix composites find applications mostly in the tissue engineering industry. Typically, PVA is used as a matrix for impregnation of reinforcements to form, for example, hydrogels, due to the ability to dissolve this material in water and obtain a good distribution of the reinforcement throughout its volume. PVA in the form of a hydrogel has low mechanical properties, but its tensile strength may increase significantly with the addition of reinforcements. Zhang *et al.* [114] *produced* PVA composite hydrogels reinforced with graphene oxide and showed the increase of the mechanical properties with the graphene oxide content increase, suggesting the excellent stress transfer between the PVA matrix and GO. It was also found that the GO content increase did not affect the hydrogel toxicity, so this composite has great potential for biomedical applications [109].

PVA matrix composites are used in membranes to control gas permeability, for gases such as O_2, H_2O, N_2 and He, in implants for replacement of damaged joints, as well as for wound dressings, in order to maintain the moisture at the surface, providing an ideal environment to clean the wound and to promote the cicatrisation process. In 2012, H. Huang *et al.* [115] investigated the permeability of PVA reinforced with graphene oxide nanoparticles (GONS) films, produced by solution blending, to oxygen and water. Figure 12 show the results obtained. It was found that both oxygen and water vapor permeability coefficients of films declined by about 98% and 68% at a low GONS loading of 0.72 vol%. The excellent results were attributed to the excellent barrier properties of GONS, their full exfoliation, uniform dispersion, high alignment in the PVA matrix and the strong interfacial adhesion between GONSs and PVA matrix [110].
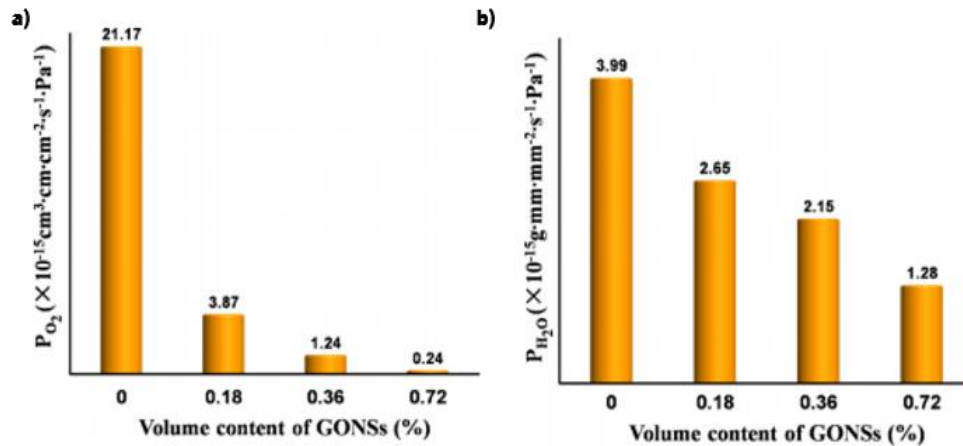
Figure 12: *Permeability coefficient of a) $O_2(P_{O2})$ and b) H_2O (P_{H2O}) for GONS/PVA nanocomposite films as a function of GONS loadings* [115].

Regarding PVA/graphene composites produced by spray coating, the literature is scarce, and only a few studies of the production of PVA composites with carbon nanotubes [101,116], SiO_2 [117] and cellulose [118] are found. PVA nanocomposites exhibit superior mechanical properties compared to the neat polymer and to the other polymer matrices composites. Table 1 clearly shows the number of studies of different polymer matrices. There was no significant improvement in the mechanical properties of the nanocomposites prepared by the spray coating process compared to the others. Graphene derivatives-based polymer nanocomposites exhibited a several fold increase in electrical conductivity. The appreciable improvement in electrical conductivity is due to the formation of a conducting network by the reinforcing particles in the polymer matrix. A close inspection of Table 1 clearly shows significant changes in electrical properties according to the polymer matrix, processing method and filler type. The maximum or very high electrical conductivity was obtained using a high carbon nanotubes loading in PVA matrices compared to other carbon fillers. Improvement in the mechanical, thermal and electrical properties of polymer nanocomposites is not only dependent on the properties of the reinforcing materials but also on the properties of the host polymer matrices. As a result, the degree of improvement in all these properties varies for different nanocomposites. The processing methods also play a significant role towards the improvement of these properties.

Various techniques have been used to produce these composite films, but the most common method is solution casting because it is a simple, fast and low consumption and low waste production technique.

The literature review summary described in Table 1 shows that for small reinforcement loads the increase in mechanical and electrical properties was significant to the point of making these composite

materials promising for supercapacitor applications [100]. As the reinforcement load increases, the properties of the composite produced improve, however, this improvement tends to a critical value, at which properties remain or even decrease.

The improvement of tensile strength with the graphene content was studied by Zhao et al. [119], reporting a significant enhancement of the mechanical properties of graphene/PVA composites with graphene loads up to 1.8 vol%. Figure 13 represents the stress-strain curves obtained and the results for the mechanical properties, showing that at 1.8 vol% of graphene loading an improvement of 150% in tensile strength was observed. The authors reported a nearly 10 times increase in Young's modulus at this graphene concentration.
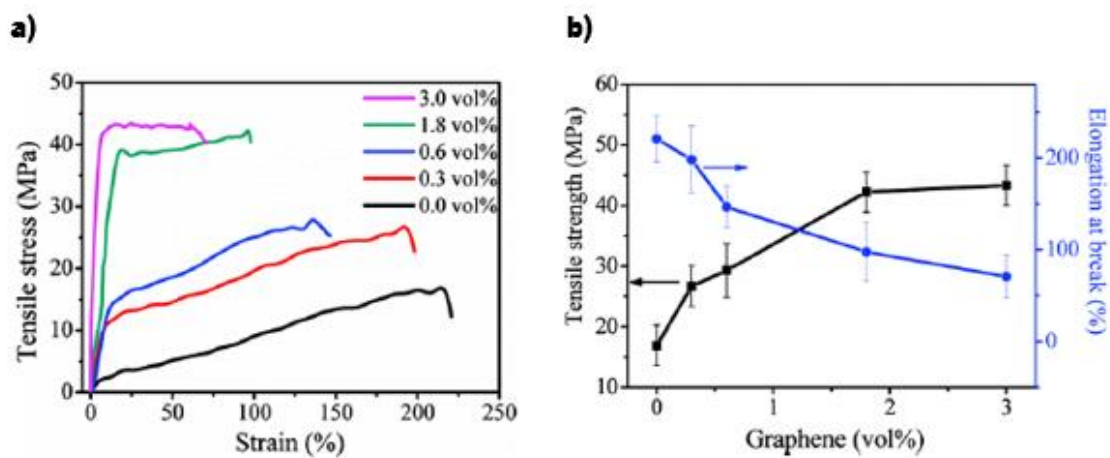
Figure 13: Mechanical properties of PVA/graphene composite films with varying graphene loadings: a) Stress-strain curves and b) tensile strength and elongation at break [119]

In terms of electrical properties, the reinforcement content will improve the conductivity of the PVA composites. Wang *et al.* [120] reports the influence of reduced graphene oxide content in the reinforcement of PVA matrix. Due to the exceptionally high conductivity of methacryloxyethyltrimethyl ammonium chloride - reduced graphene oxide (DMC-rGO) the investigators expect the composite to present high electrical conductivity. According to the Figure 14 the addition of rGO has a considerable influence in the electrical properties, increasing the conductivity of the corresponding composites. Conductive pathways can be formed with low DMC-rGO loading, increasing the electrical conductivity of the composite for DMC-rGO loading of 2 vol %, reaching six orders of magnitude greater than that of pure PVA.
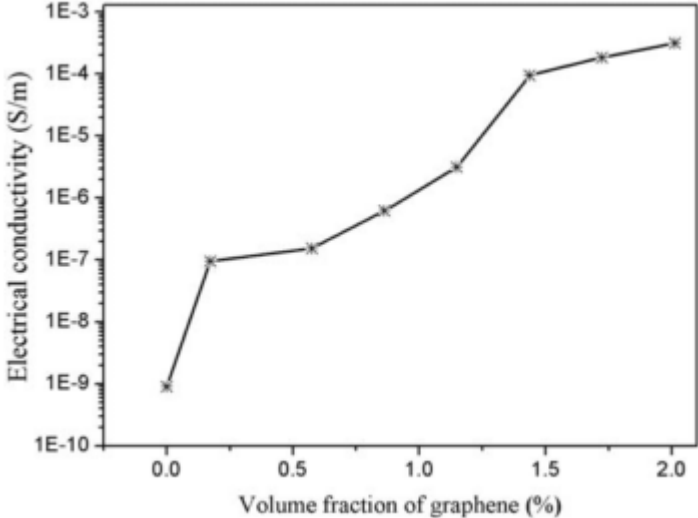
Figure 14: *Electrical conductivity of DMC-rGO/PVA composites as function of DMC-rGO content* [120].

CHAPTER 2.

MATERIALS AND METHODS

2. MATERIALS AND METHODS

In this chapter it will be described the materials and experimental methods used during the present work in order to produce functionalized few-layer graphene and composite films.

2.1. Materials

In this work, the composite films were produced from Polyvinyl alcohol (PVA) as their matrix and graphite as reinforcement. PVA was purchased from Hainan Huarong Chemical Co.,Ltd, with a hydrolysis degree of 88% and more than 93.5 of purity. Graphite Micrograf HC11 was provided by Nacional de Grafite, Brasil, is a micronized graphite, with 99.5% purity and median particle diameter (d_{50}) of 11 μm. The nomenclature adopted in this work is Micrograf. The non-covalent functionalization of graphite was achieved using a pyrene derivative synthesized in the laboratory and distilled water. The structure of the pyrene derivative is represented in Figure 15.
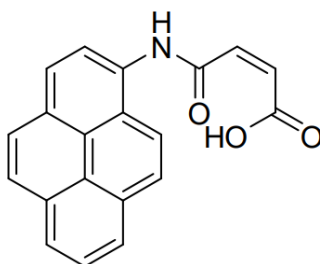
Figure 15: *Molecular structure of pyrene derivative*

2.2. Methods

2.2.1. Production of functionalized few layer graphene suspensions

The functionalization of few-layer graphene was performed through a non-covalent method, stabilizer-assisted liquid phase exfoliation.

Firstly, a pyrene-derivative (PY) solution was prepared by adding 7.9 mg to 500 ml of ultra-pure water. The concentration of the solution was $5x10^{-5}$ mol/dm^3 and to assure the total dissolution of PY it was necessary to adjust the pH to 7 by using a solution of potassium hydroxide (KOH) 1M, then ultrasounds were applied to the solution during 2h.

The graphite was functionalized and exfoliated by preparing a suspension of 0.250 g of graphite in the PY solution. The suspension was exposed to an Ultrasonic processor UP100H from Hielscher,

equipped with a sonotrode MS14D, as shown in Figure 16. Ultrasound energy was applied to the suspension during 3h. During the process, PY adsorbs to the graphene layers of graphite, aiding exfoliation and maintaining the few-layer graphene formed stable in the solution, preventing their restacking.
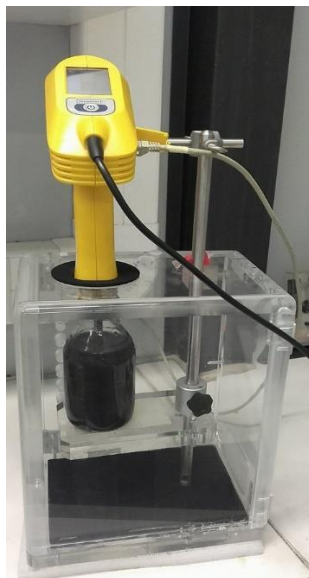
Figure 16: *Equipment used to produce functionalized FLG suspensions*

After sonication, the functionalized few-layer graphene suspension was centrifuged in Heraeus Megafuge16 at 5500 rpm during 1h, to remove the larger aggregates and the supernatant was collected.

2.2.2. Production of PVA solutions

To perform the spray coating experiments, it was necessary to produce PVA solutions. The solutions were prepared with various concentrations in order to test the maximum viscosity that it's possible to have in PVA solutions to produce PVA films with good quality.

PVA was dissolved in ultra-pure water by magnetic stirring, during 5h at a temperature of 110°C. Initially the PVA concentration of the solutions prepared were 60 mg·ml, 120 mg·ml, 180 mg·ml and 250 mg·ml. Then, more two solutions with different PVA concentrations were prepared, 135 mg·ml and 150 mg·ml, because it's too difficult to spray the solutions with 180 and 250 mg·ml, as its viscosity is too high to use in Airbrush gun.

Thereafter, the PVA films produced with the solution of 150 mg·ml presented a lot of air bubbles. This problem was not observed with the solution of 135 mg·ml. So, the maximum concentration used to produce the PVA composite films was 135 mg·ml.

In order to investigate the exfoliation degree of graphite in PVA films, it was necessary to prepare two types of solutions. One was prepared through the water suspensions of FLG obtained from Micrograf that was mixed with PVA using magnetic stirring, during 5h at a temperature of $110°C$. The other solution was prepared by adding graphite powder and PVA to a flask with ultra-pure water, which was stirred until all the PVA was dissolved.

To compare the results of composite films with non-exfoliated and exfoliated graphite and to verify the effect of the incorporation of graphite, pure PVA control films were produced.

2.2.3. Production of PVA composite films

Spray coating is an extremely versatile technique used to coat surfaces and to produce nanostructured polymeric films. Pneumatic-based systems use a current of pressurized air or gas that divide the liquid into small droplets at the nozzle. The main parameters for the atomization process are surface tension, viscosity, fluid density, gas flow properties, and nozzle design. The quality of the coated layer is defined by the wetting behaviour, surface properties, working distance, coating speed, droplet sizes and the number of sprayed layers. Besides the solution-surface interaction the kinetic impact of the droplets influences the spreading of the droplets. The temperature of the surface has also an important role for the quality of the sprayed surface. The simplest form of a pneumatic-based system is an airbrush gun.

In this work, it was necessary to proceed to some adjustments in the spray system to operate the airbrush correctly and to produce films with good quality. Table 2 describes the operatory conditions that were varied to produce PVA films and the output observed.

After this optimization step it was found that the more adequate conditions were the following: PS substrate, substrate temperature of $60°C$, pressure of 2 bar and maximum throughput. The films were produced using the referred parameters.

Table 2: Optimization of spray coating technique for PVA films

Substrate	Substrate Temperature (°C)	Pressure (bar)	Throughput	Behaviour
PS (semicrystalline)	100	1	Max.	Damaged substrate
		2	Max.	Damaged substrate
PE (film)	100	1	Max.	Damaged substrate
		2	Max.	Damaged substrate
Glass	100	1	Max.	PVA adheres to the substrate
		2	Max.	PVA adheres to the substrate
Steel	100	1	Max.	PVA adheres to the substrate
		2	Max.	PVA adheres to the substrate
PS (Amorphous)	100	1	Max.	Films with many air bubbles
		1	Med.	Films with many air bubbles
		2	Max.	Films with many air bubbles
		2	Med.	Films with many air bubbles
	60	1	Max.	Long spray time
		1	Med.	Long spray time
		2	Max.	Films with good quality
		2	Med.	Films with good quality

The composite films production was performed with an airbrush (RONGPENG-RP8816/PB-381). Before the production of PVA composite films, it was necessary to prepare the solutions as referred in 4.2.3. and place the PS substrate on a heat plate at a temperature of 60°C.

Then, 6 ml of each solution was placed in the airbrush. The spray system was maintained at 15 cm height from the substrate. After that, the substrate was removed from the heat plate and placed in a flat table overnight. The drying was finished at room temperature until the detachment of the films from the substrate was possible. The heat plate and the spray system used to produce PVA composite films are shown in Figure 17.

Figure 17: Equipment used to produce PVA composite films

2.3.   Characterization of composite films

2.3.1. Water Vapor Transmission test

Water vapor transmission (WVT) test consist in the determination of water vapor flow per unit time through unit area of a flat material. The study of WVT was carried by a desiccant method according to ASTM E96 standard. Before starting the procedure of samples preparation, the thickness of films was measured at four different points with the help of a digital micrometre (*Mitutoyo*). Then, the films were placed over aluminium dishes containing silica gel and fixed with an aluminium ring, sealed with melted pure paraffin, according to the specification of the standard. Finally, the samples were placed in a desiccator, containing 18% H_2SO_4 solution in ultrapure water and then, the desiccator was placed in an oven with a controlled temperature at 38°C.

Water vapor transmission, WVT [g/h·m^2] of the samples was calculated using equation 1.

$$WVT = G/tA = (G/t)/A \tag{1}$$

Where, G [g] is the weight variation of the aluminium cups along the time of exposure to water vapor, t [h] the time during which exposure occurred and A [m^2] the exposed film area.

Then, permeance [g/Pa·s·m^2] was obtained using equation 2.

$$Permeance = WVT/\Delta p = WVT/S(R1 - R2) \tag{2}$$

Where, Δp [Pa] is the vapor pressure difference, in mm Hg (1.333 X 10^2 Pa);

S [Pa] is the saturation vapor pressure at test temperature;

R$_1$ is the relative humidity in the chamber (90%) and R$_2$ the relative humidity in the vapor sink (inside the aluminium cups,0%).

In this work the temperature used was 38°C, so the S value is considered to be 49.692 mmHg.

The water vapor permeability coefficient, P(H$_2$O), was calculated according to the equation 3.

$$P(H_2O) = Permeance \times thickness \tag{3}$$

Thickness [m] is the thickness of films.
All results obtained result from three different tests for each composition.

2.3.2. Electrical Conductivity measurements

Since 1960 it is known that the effects of electrical stimuli on tissues can influence cellular behaviour and function [116]. Through the utilization of external electrical stimuli, it's possible to gain greater control over cellular growth, maturation, adhesion, and orientation. *In vivo* environment, by taking electricity into account when growing tissue constructs, it´s possible to significantly improve the quality of the tissue-engineered product [117].

In this work, a picoammeter Keithley Instruments Inc., model 6487 was used to determine the electrical conductivity of composite films. Current intensity measurements were performed using direct current, changing the applied voltage between -10.0 and 10.0 V. The test samples were rectangular with an area of $1x10^{-4}$ m^2. The thickness was measured before the test using a micrometre (*Mitutoyo, Japan*).

The resistance, R [Ω], of the samples was determined through Ohm's law, equation 4.

$$V = RI \tag{4}$$

Where, V [V] is the voltage applied and I [A] the current measured.

Then, to determine the volumetric resistivity, ρ_V [Ω·m], it was used the equation 5.

$$\rho_V = \frac{A}{t}R \tag{5}$$

Where, A [m^2] is the superficial area of samples/electrode, t [m] the thickness of samples and R [Ω] the resistance determined above.

Finally, the volumetric electrical conductivity, σ [S/m] is the reciprocal of volumetric resistivity, equation 6.

$$\sigma_V = \frac{1}{\rho_V} \qquad (6)$$

All results obtained result from five different tests for each composition.

2.3.3. Raman Spectroscopy

Raman spectroscopy is a scattering technique, based on Raman Effect, i.e., frequency of a small fraction of scattered radiation. In Raman spectroscopy, sample is illuminated with a monochromatic laser beam which interacts with the molecules of sample and originates a scattered light [118]. The scattered light having a frequency different from that of incident light is used to construct a Raman spectrum.

Raman spectroscopy test was performed to verify the presence of graphite in composite films. The composite films, graphite and functionalized graphene powders were placed on a glass coverslip and then analysed on a LabRAM HR Evolution Raman Microscope Horiba Scientific, under a laser excitation wavelength of 532 nm. The results were analysed with a LabSpec6 software.

2.3.4. Thermogravimetric Analysis (TGA)

Thermogravimetric analysis (TGA) has appeared as powerful technique to monitor physical and chemical changes in materials. This method measures the amount and rate of change in the weight of a material as a function of temperature or time in a controlled atmosphere. Measurements are used primarily to determine the composition of materials and to predict their thermal stability at high temperatures. The technique can characterize materials that exhibit weight loss or gain due to decomposition, oxidation or dehydration.

This technique that can be used in various applications, for example, to study the thermal stability of materials in a large scale of temperatures, which is very important because it can predict the lifetime of materials under certain temperature. It can be also performed to test the composition, kinetics features of weight loss or gain through controlling the chemistry and the corrosion of materials in contact with other reactive gases.

Chapter 2. Materials and Methods

TGA analyses were performed to evaluate the thermal stability of PVA, PVA/G and PVA/EG films and to determine the amount of graphite and graphene products incorporated in the composite films. The TGA assays were performed on a Q500 equipment (TA Instruments, USA) under nitrogen atmosphere, within a temperature range from 60°C to 700°C. The experiments were run at a scanning rate of 10 °C/min.

2.3.5. Differential Scanning Calorimetry (DSC)

Differential scanning calorimetry (DSC) is one of the thermo-analytical techniques used to measure changes in heat flows with material transitions. DSC measurements provide both qualitative and quantitative data on endothermic and exothermic processes. If the sample absorbs heat it undergoes to an endothermic phase transition, if the sample has a heat evolving it undergoes to an exothermic process. DSC is commonly used to determine the glass transition and melting temperatures of polymeric materials.

DSC assays were performed on a DSC 200 F3 Maia (Netzsch) under nitrogen atmosphere and heating/cooling speed of 10°C/min. PVA, PVA/G and PVA/EG samples were firstly submitted to a heating cycle within a temperature range from 20°C to 220°C and then an isothermal stage of 2 min at 220°C. After this step, the samples were subjected to a cooling cycle from 220°C to 20°C and also to an isothermal stage during 2 min at 20°C. Finally, it was proceeded to a second heating cycle with the same temperature range of the first heating.

DSC analysis were performed to evaluate the glass transition temperature, T_g, heat capacity, ΔCp, melting temperature, T_f, and melting enthalpy, ΔH_f. These values were calculated through the software Proteus da Netzsch.

The crystallinity degree, χ_c [%], was obtained through equation 7.

$$\chi_c = \frac{\Delta H_f}{\Delta H_f^0} \times 100 \tag{7}$$

Where, ΔH_f [J/g] is the enthalpy of fusion of PVA sample and ΔH_f^0 [J/g] is the melting enthalpy of PVA with a crystallinity degree of 100%, that is 138.6 J/g [92].

For the composite films, the crystallinity degree is calculated by the equation 8.

$$\chi_c = \frac{\Delta H_f}{\Delta H_f^0 \times (1 - \emptyset)} \times 100 \tag{8}$$

Where Ø is the mass fraction of the graphite and exfoliated graphite particles presented in composite films.

All the results are an average of three tests for each composition.

2.3.6. Scanning Electron Microscopy (SEM)

Scanning Electron microscopy is one of the most used techniques in science field. It's performed at high magnifications, generates high-resolution images, examines the surface microstructure morphology, local chemical composition, crystalline structure and orientation of materials. The operating system is based on a focused beam of high-energy electrons to generate a variety of signals at the surface of samples. The samples are under vacuum to ensure the electron beam stays focused and does not interact with particles in the air. When the beam of electrons hits the sample, it causes secondary electrons to be released from the sample which are detected to provide an image based on the topography of the surface. The most commonly used detectors are the Secondary Electron Detector (SED) and the Backscattered Electron (BSE) Detector and with the interaction between the electrons and the detector it's possible to create an image [120,121].

SEM analysis were performed on NanoSEM-FEI Nova 200 to characterize the morphology of composite films and the dispersion of particles thorough the PVA matrix. To observe the cross-section, the samples were fractured using liquid nitrogen. Before the analysis the samples were submersed in liquid nitrogen to obtain a fragile fracture at low temperatures. To analyse the morphology, the composite films were fixed in an aluminium support and then coated with Au-Pd (gold-palladium) layer, to make the samples electrically conductive.

2.3.7. Mechanical Characterization – Uniaxial Tensile tests

Understanding material mechanics is very important for tissue engineering because it can provide one of the most common cause of failure, that is related to the mechanical mismatch between the graft and the host tissue. The uniaxial tensile tests provide a simple and effective way to characterize the material response to loading. By subjecting a sample to a controlled displacement along a single axis, the change in dimensions and resulting load can be recorded to calculate a stress-strain curve. Through the obtained curve, it's possible to determine the elastic and plastic material properties, such as Young's modulus, yield stress, ultimate tensile strength, elongation at break [122].

Chapter 2. Materials and Methods

The uniaxial tensile tests were performed to evaluate the mechanical properties of composite films, following ASTM D882 norm, using an Instron 5969 at room temperature of 25°C, using a load cell of 1kN under load speed of 5mm/min and a gauge length of 30 mm. Before proceeding to the assays, the samples were prepared by cutting the films in rectangular pieces with 5mm width and 50mm length, then they were placed in a paper frame to reduce the films manipulation and prevent the damage of films by the tensile machine ties. In Figure 18 is represented the samples used in uniaxial tensile tests with their respective measures. The thickness of composite films was determined in three different regions of each sample using a micrometer (Mitutoyo, Japan).
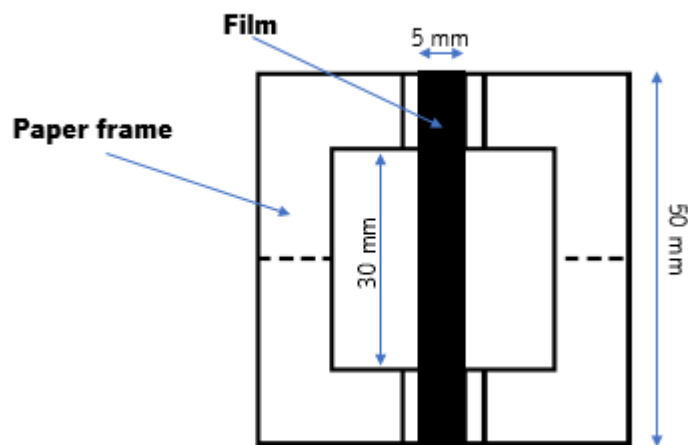
Figure 18: *Representation of the paper frame and the film samples used in uniaxial tensile tests*

The results provided by the equipment of tensile tests are force-displacement curves so, to determine the ultimate tensile strength, elongation at break, and Young's modulus it's necessary to perform some auxiliary calculations to obtain stress-strain curves.

The tension, σ [MPa] is obtained by the equation (9.

$$\sigma = \frac{F}{A} \tag{9}$$

Where A[mm^2] is the cross-section area, that is corrected by the thickness and width of each sample.

Deformation, ε [%] is determined by the equation (10.

$$\varepsilon = \frac{\Delta l}{L} \tag{10}$$

Where, Δl[mm] is the displacement and the L[mm] is the distance between ties.

After the calculations, the stress-strain curves are achieved by using the software Origin. The values obtained result from an average of five different samples from each composition.

2.3.8. Ultraviolet-Visible (UV-Vis) Spectroscopy

Ultraviolet-Visible (UV-Vis) Spectroscopy is one of the most omnipresent analytical and characterization techniques in science. This technique can be employed in many applications and doesn't have any other rival technique because of its simplicity, versatility, speed, accuracy and cost-effectiveness.

The operating principle of this instrument is relatively simple. For a double-beam UV-Vis spectrophotometer, the functioning system consist in a beam of light from a visible or UV light source that is separated into its component wavelengths by a prism. Each single wavelength beam is divided in two equal intensity beams. One beam passes through a cuvette containing a solution of the compound being analysed in a transparent solvent (sample). The other beam passes through an identical cuvette containing only the solvent (reference). The intensities of these light beams are then measured by electronic detectors and then they are compared. The intensity of the reference beam is defined as I_0. The intensity of the sample beam is defined as I. Over a short period of time, the spectrometer automatically scans all the component wavelengths in the manner described [123].

$$A = log_{10}\frac{I_0}{I}$$

(11)

For a single-beam UV-Vis spectrophotometer, the functioning system consist firstly in a measure of the absorption of the solvent (reference), and then the absorption of the solution (sample). The ultraviolet (UV) region scanned is normally from 200 to 400 nm, and the visible is from 400 to 800 nm. This was the approach used in the present work [123].

To determine the concentration of the solutions, the Beer-Lambert law was used, equation (12.

$$A = \varepsilon lc$$

(12)

Where, ε [$cm^2 \cdot g^{-1}$] is the absorptivity coefficient, l[cm] is the width of the cuvette that contains the solution and c[$g \cdot cm^{-3}$] the solution concentration. The application of this equation is limited to dilute

solutions, because it is only valid to measure the concentration of dilute solutions since ε is independent of the concentration of the solution at a given wavenumber only when the absorbance is lower than 1 [124].

UV-vis spectroscopy analysis was performed in a UV-2401 PC equipment (Shimadzu, Japan), in order to quantify the exfoliated graphite concentration present in solution. The assays were carried out in a quartz cells and several dilutions was necessary to be possible to obtain non-saturated spectrum.

CHAPTER 3.

RESULTS AND DISCUSSION

3. RESULTS AND DISCUSSION

3.1. Production of PVA composite films

The Micrograf suspensions were mixed with polyvinyl alcohol. Thin films with 0.5 wt.%, 1 wt.%, 3 wt.% and 5 wt.% of exfoliated and non-exfoliated graphite were prepared. PVA control films were also prepared for the sake of comparison. The samples name used in this work is presented in Table 3. The weight content of the composite films was changed to the values obtained on the real weight column of Table 4 of TGA assays. The reason of the difference in the weight content values between the expected and the real loading levels of the composites is discussed in section 3.3.3..

Table 3: Real weight content and designation of samples with the values obtained for TGA assays

Materials	Weight content (wt%)	Sample Name
PVA	—	PVA
PVA + Graphite	0.4	PVA/Micrograf 0,4%
	0.8	PVA/Micrograf 0,8%
	1.5	PVA/Micrograf 1,5%
	2.2	PVA/Micrograf 2,2%
PVA + Graphite + Pyrene	0.5	PVA/Micrograf PY 0,5%
	2.2	PVA/Micrograf PY 2,2%
	6.1	PVA/Micrograf PY 6,1%
	9.3	PVA/Micrograf PY 9,3%

The control films and the films produced with exfoliated and non-exfoliated graphite are shown in Figure 20. The PVA films were transparent while the composites had a grey colour that became darker with the increase of Micrograf concentration. All the films exhibited thickness ranging from 40μm to 50μm. The images of the films are divided in two zones, Zone A (center zone of the films) and Zone B (extremity of the films) to evidence the graphite gradient. Figure 19 shows a film with the representation of the two zones, A and B and with an example of the place where samples were removed in order to perform the characterizations techniques.
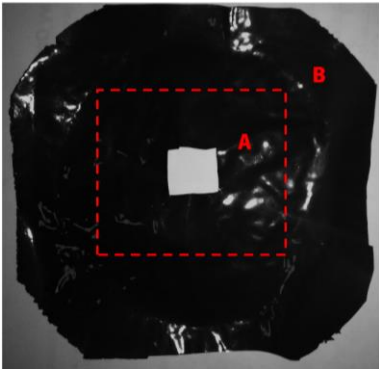
Figure 19: Film divided two zones, A and B with a sample removed from the center zone

The films with reinforcement content until 2.2% show a gradient of particles through the entire film, being higher in the extremities, and it's also possible to observe in some films the formation of agglomerates. For films with reinforcement content higher than 2.2%, it's not possible to detect the same gradient at the macroscopic scale.
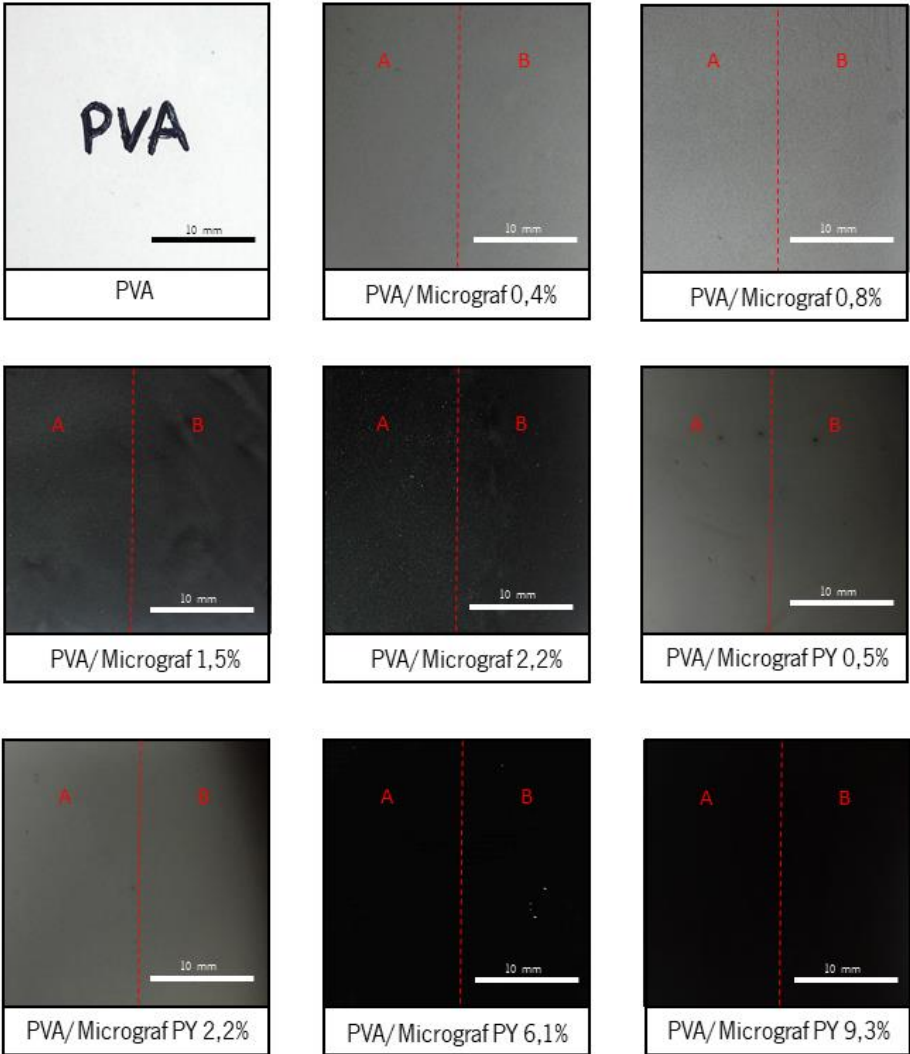
Figure 20: Macroscopic representation of PVA, PVA/Micrograf and PVA/Micrograf PY composite films

3.2.   Scanning Electron Microscopy (SEM)

The morphology of the cross-section of PVA, PVA/Micrograf and PVA/Micrograf PY films was analysed through SEM. Figure 21 show the images obtained for the cross sections of PVA and the composites with 0.8 and 2.2 wt% graphite and 2.2 and 9.3 wt% of exfoliated graphite. In general, it can be seen that PVA/Micrograf films present an heterogenous distribution of graphite whereas PVA/Micrograf PY are quite homogenous.

Figure 21 shows that for PVA/Micrograf films, the graphite particles were deposited and accumulated onto the surface in contact with the substrate used for their production, due to the large dimensions of graphite particles. PVA/Micrograf 2.2% show graphite particles with small dimensions dispersed through the film volume. Regarding the dispersion loads of 0.8 and 2.2 wt%, it's possible to observe that for 0.8 wt% of non-exfoliated graphite the lower surface has less accumulation, because of the weight content of graphite added to the PVA solution. Arantes report the same occurrence, i.e, the deposition and the presence of particles with different dimensions, for PVA/Micrograf films with various weight contents produced by solvent casting [125].

For PVA films reinforced with exfoliated graphite (Figure 22), the presence of particles with small dimension is well visible, which means that the exfoliation of graphite has a significant influence in the size reduction of graphene sheets. This phenomenon is more visible in the composite with 9.3 wt% exfoliated graphite in which more particles are dispersed along the cross-section. Liang *et al.* [92] also proceed to the exfoliation of graphene oxide, in order to obtain GO particles with small size and to have a stable GO/H_2O solution. They produced PVA/GO films through solvent casting and reported that such GO sheets were clearly well-dispersed in the PVA matrix. The homogeneity of PVA/Micrograf PY films found in the present work is also due to the used spray coating technique, so with this technique it's possible to obtain composite films with excellent properties, like transmittance strain sensing property as reported by Liu and Zhang [126]. Moreover, this technique is fast, scalable and easy to operate.

Comparing PVA/Micrograf and PVA/Micrograf PY films, it's observed that graphite and exfoliated graphite have excellent stability in PVA solution and good interaction with the polymer. By observing the SEM images with a magnification of 50000x it is clear that the surfaces of protruding graphite and EG sheets were coated with PVA. So, strong interfacial interactions between the reinforcements and the polymer matrix were established. Xu *et al.* found the same behaviour for PVA/GO films [127].
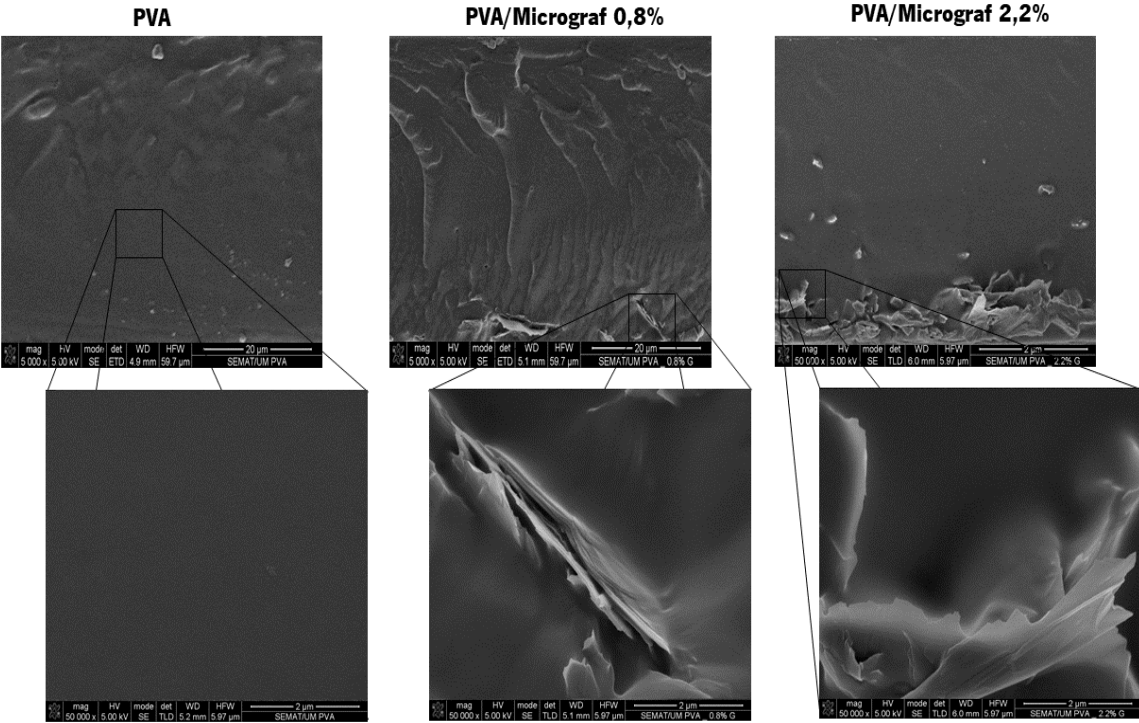
Figure 21: Images obtained by SEM of PVA, PVA/Micrograf 0.8% and PVA/Micrograf 2.2%
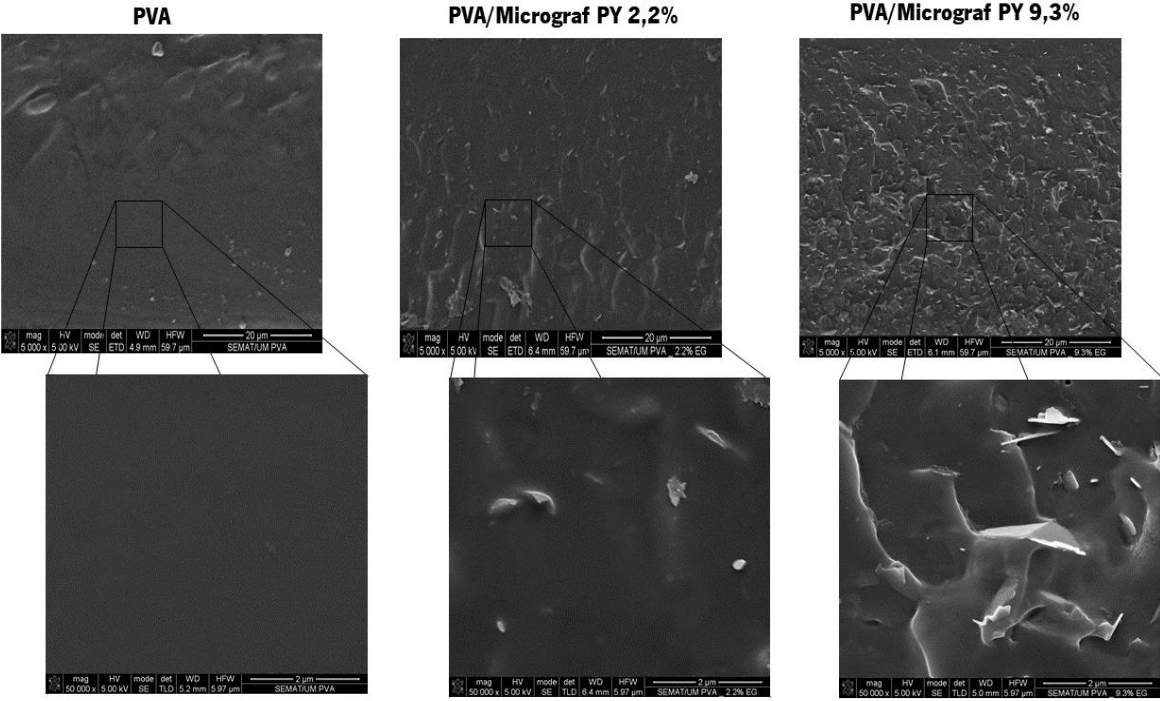
Figure 22: Images obtained by SEM of PVA, PVA/Micrograf PY 2.2% and PVA/Micrograf PY 9.3%

3.3. Thermogravimetric Analysis (TGA)

3.3.1. Powders

The TGA results of graphite and exfoliated graphite powder, as well as the PY used for the functionalization of graphite, are presented in Figure 23. PY presents the lowest thermal stability, starting the thermal degradation above approximately 150 °C and presenting a weight loss of 79 wt%. The weight loss observed for the pristine graphite is small and mainly due to the release of adsorbed water. Parviz *et al.* reported the same behaviour [56].

Micrograf is thermally stable across the temperature range, resulting in only 0.53 wt% of weight loss. For functionalized Micrograf with PY, the thermal stability decreases reaching a weight loss of 29.3wt% at 700 °C.
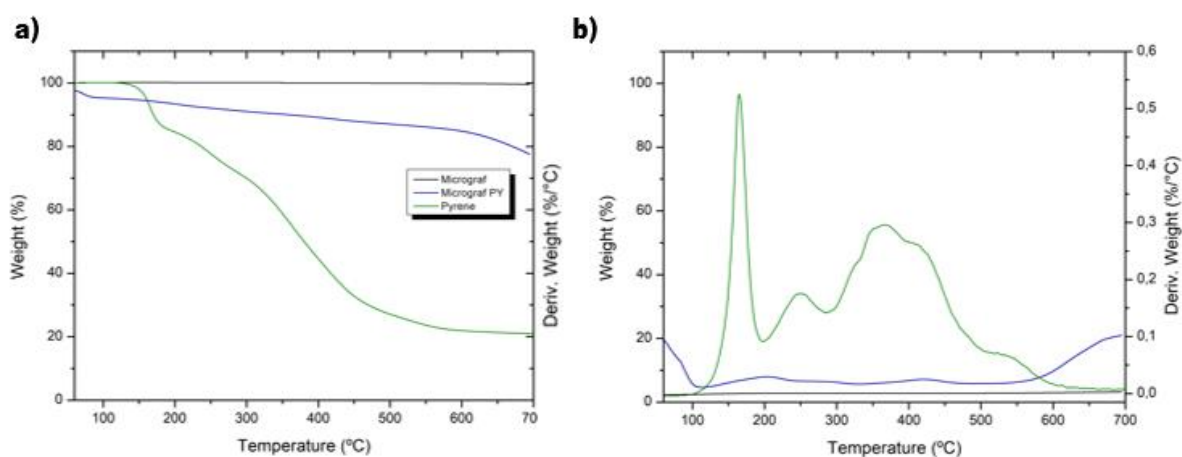
Figure 23: *TGA analysis of a) Pyrene, Micrograf and Micrograf PY and b) respective Deriv. Weight*

3.3.2. PVA composite films

The thermal stability of PVA composite films was evaluated by TGA and the weight percentage of exfoliated graphite incorporated in the composite films was determined. TGA assays were performed on samples removed from the center (Zone A) and the extremities (Zone B), with the aim of evaluating the particles dispersion through the films volume. Thereafter, the other characterization techniques were performed with samples removed only from the Zone A of films, so the discussion of TGA results was relative to the results obtained in this zone. The results of TGA assays for samples removed from zone B was presented in Anexo II. The results illustrated in Figure 24 indicated that for PVA and PVA/Micrograf films no modification was observed in the degradation temperature with the increase of Micrograf content.
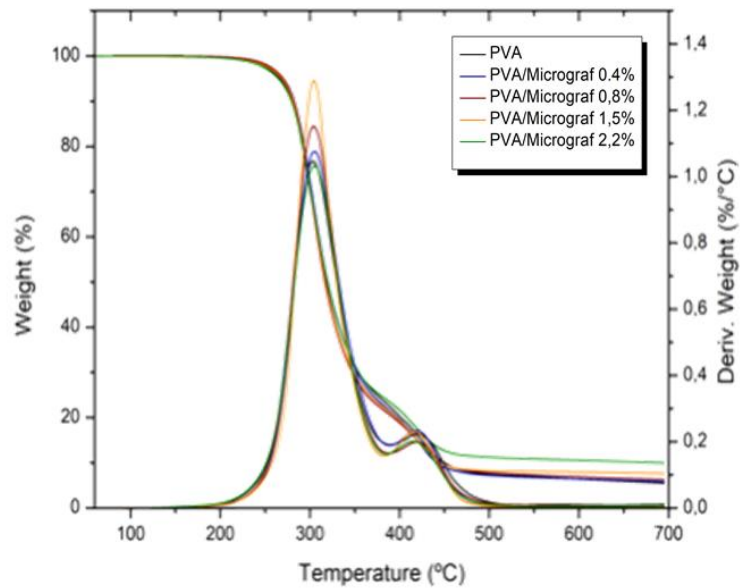
Figure 24: *TGA curves of the PVA/Micrograf films and their respective weight derivate curve for samples removed from a) zone A; and b) zone B.*

The TGA data of PVA and PVA composites reinforced with exfoliated graphite are shown in Figure 25. The results indicated that for TGA assays made in samples removed from the center of the films the degradation temperature has a significant decrease with the increase of exfoliated graphite weight. When compared to the control films, PVA and for example PVA/Micrograf 2.2% with initial degradation temperature of 279.42°C and 274.40°C respectively, the temperature decreased to values of 269.70°C for 2.2 wt% of exfoliated graphite.
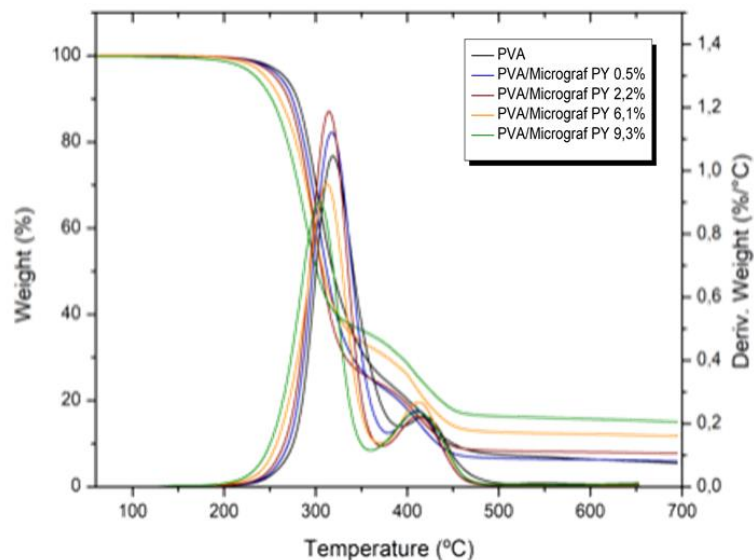
Figure 25: *TGA curves of PVA/Micrograf PY films and their respective weight derivate curve for samples removed from a) zone A; and b) zone B.*

The TGA results obtained in Figure 24 and Figure 25 show that the degradation of PVA and composites starts at 200°C. The weight loss is observed between 200 °C and 500 °C, due to the

dehydration and the formation of volatile products followed by the bond scission in the polymeric backbone and the PY used for the Micrograf functionalization, as reported by Galotto and Ulloa [128]. Above 500 °C, the weight loss tends to stabilize, leaving a residual weight from the decomposition of polymer backbone, from graphite, for composite films with graphite, and also from the graphene-based material, for the films with exfoliated graphite. A similar result was observed by Cao *et al.* [129] for composites based on PVA and graphene derivates. PVA/Micrograf PY films have higher residual weight compared to the PVA and PVA Micrograf films, because graphene-based material has much higher thermal stability under inert atmosphere, so they leave higher residual weight.

The residue values of PVA, PVA/Micrograf and PVA/Micrograf PY films are presented on Table 4 and Table 5 as well as the estimated weight content. The weight content in both tables has a deviation from the nominal value of weight content of PVA composite films, being that in Table 5 the values were much higher than expected. The difference in weight content between the samples removed from the center and the extremities reveals the heterogeneity of the films along the surface, already evidenced in Figure 22 due to a problem with the substrate danification.

Table 4: *Values obtained from TGA assays on Zone A*

	Weight content (wt%)	Residue (%)	Weight Loss (%)	T_{onset} (°C)	T_{max} (°C)	Real Weight (%)
PVA	-	5.48	94.48	279.42	302.78	
PVA/Micrograf	0.4	5.86	94.19	277.72	304.52	0.4
	0.8	6.32	93.76	278.24	303.9	0.84
	1.5	7.03	93.05	275.42	303.64	1.54
	2.2	7.68	90.06	274.4	304.61	2.18
PVA/Micrograf PY	0.5	5.95	94.09	272.28	301.41	0.45
	2.2	7.74	92.35	269.7	298.01	2.2
	6.1	11.78	88.34	262.21	295.42	6.12
	9.3	15.06	84.67	251.28	285.36	9.31

Table 5: Values obtained from TGA assays on Zone B

	Weight content (wt%)	Residue (%)	Weight Loss (%)	T_{onset} (°C)	T_{max} (°C)	Real Weight (%)
PVA	-	3.26	95.99	293.21	320.45	
PVA/Micrograf	0.4	4.16	95.83	277.39	305.05	0.89
	0.8	4.43	95.42	275.67	302.18	1.16
	1.5	7.04	93.05	275.42	303.64	3.75
	2.2	7.38	92.28	283.7	318.03	4.1
PVA/Micrograf PY	0.5	5.04	95.08	268.04	295.01	1.67
	2.2	9.72	89.68	272.44	310.85	6.08
	6.1	12.02	87.46	258.03	292.21	8.23
	9.3	14.55	85.45	287.93	246.35	10.61

3.4. Water Vapor Transmission

The results of water vapor transmission (WVT) assays for PVA, PVA/Micrograf and PVA/Micrograf PY, are presented in Figure 26. Owing to the hydrophilicity of abundant hydroxyl groups on PVA molecular chains, the barrier properties of PVA film will be greatly influenced by water vapor. The values obtained in WVT assays were an average of three samples for all the formulations.

Compared with pure PVA films, the water vapor permeability of PVA/Micrograf and PVA/Micrograf PY composites declines significantly for low reinforcement content. The $P(H_2O)$ decreases from 6.51×10^{-5} (s/Pa·s·m^2·m) to 4.84×10^{-8} (s/Pa·s·m^2·m) by adding only 0.4 wt% graphite, corresponding to >99% reduction than that of pure PVA. Huang *et al.* also reported a significant reduction in water vapor permeability, but they used a different graphene derivate, GONS, to reinforce PVA [110]. The reduction achieved in water vapor permeability with graphene oxide nanosheets loading of 0.72 vol.% was decreased by approximately 68% [110].

Comparing the composite films reinforced with 0.4% wt% graphite and 0.5% wt% exfoliated graphite, the reduction in permeability coefficient was small, decreasing from 4.84×10^{-8} (s/Pa·s·m^2·m) to 3.83×10^{-8} (s/Pa·s·m^2·m), that corresponds to 21% reduction.

For weight contents of exfoliated graphite superior to 2.2 wt%, the composite films didn't improve their permeability to water vapour. This feature could be attributed to several factors: the tendency of graphene sheets to form clusters, the heterogeneity of composite films and also the films thickness (between 40 to 50 μm), because these films have a very small thickness, which the appearance of a large air bubble can cause an easy pathway to water vapor across the film.
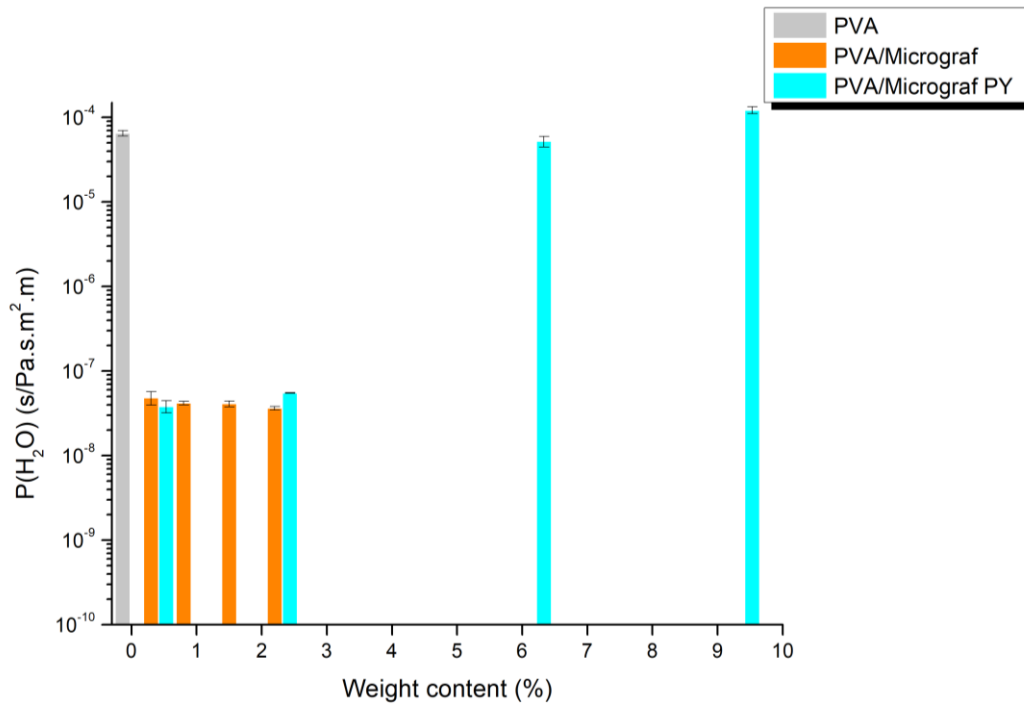
Figure 26: *Permeability coefficient of H_2O (P_{H2O}) for PVA, PVA/Micrograf and PVA/Micrograf PY films*

3.5.   Differential Scanning Calorimetry (DSC)

Differential Scanning Calorimetry (DSC) tests were carried out to study the influence of the incorporation non-exfoliated and exfoliated graphite on the thermal properties of PVA films. Figure 27 shows the first heating and cooling curves for PVA, PVA/Micrograf and PVA/Micrograf PY. In these curves it's possible to observe the variations of the glass transition temperature, cold crystallization, heat capacity, melting temperature, and melting enthalpy with the increase of graphite and exfoliated graphite weight content. It is possible to observe that the crystallization peak of PVA is not visible in the cooling curves of PVA/Micrograf PY 6.1 and 9.3%.
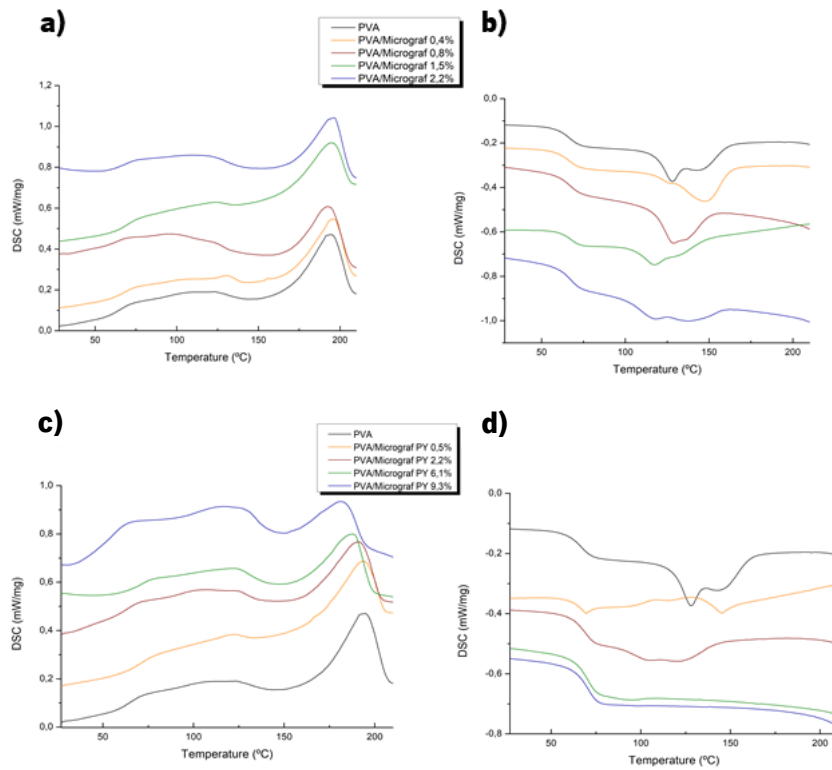
Figure 27: *First heating curves for a) PVA/Micrograf and b) PVA/Micrograf PY; and cooling curves for c) PVA/Micrograf and d) PVA/Micrograf PY films*

The second heating curves for PVA, PVA/Micrograf and PVA/Micrograf PY films are presented in Figure 28 a) and b).
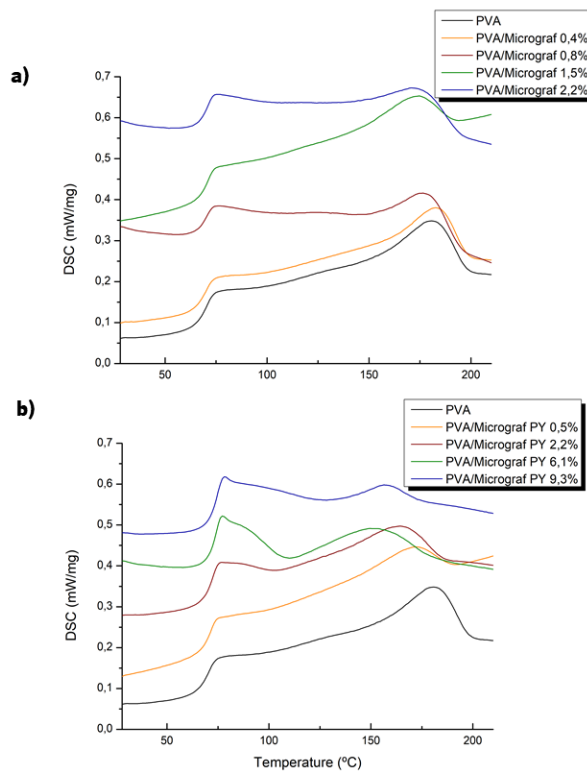
Figure 28: *Second heating curves of PVA and PVA/Micrograf PY composite films*

Chapter 3. Results and Discussion

DSC experiments allowed to calculate the melting temperature (T_m), glass transition temperature (T_g), heat capacity (ΔC_p), melting enthalpy (ΔH_f) and crystallinity degree (χ_c) of PVA and PVA composite films. These values are presented in Table 6.

Table 6: *DSC results obtained for PVA and PVA composites*

	Weight content (wt%)	T_g (°C)	ΔCp (J/g·K)	T_m (°C)	ΔH_m (J/g)	χ_c (%)
PVA	—	69.7 ± 3.2	0.284 ± 0.027	192.6 ± 3.4	39.7 ± 3.1	28.6 ± 1.3
PVA/Micrograf	0.4	61.2 ± 5.0	0.256 ± 0.063	194.7 ± 1.6	34.1 ± 0.5	24.8 ± 0.2
	0.8	64.8 ± 2.4	0.244 ± 0.077	193.4 ± 1.3	35.3 ± 1.8	25.7 ± 1.3
	1.5	65.2 ± 2.9	0.220 ± 0.067	194.1 ± 0.6	30.5 ± 2.3	22.7 ± 2.1
	2.2	65.0 ± 1.8	0.189 ± 0.035	195.0 ± 1.3	30.5 ± 1.1	23.1 ± 0.7
PVA/Micrograf PY	0.5	68.6 ± 1.1	0.220 ± 0.078	192.2 ± 1.6	27.2 ± 0.7	19.7 ± 0.5
	2.2	66.5 ± 3.6	0.256 ± 0.056	189.5 ± 1.9	31.1 ± 0.6	22.6 ± 0.2
	6.1	65.6 ± 4.6	0.274 ± 0.061	186.2 ± 1.0	25.2 ± 1.6	18.7 ± 1.1
	9.3	49.4 ± 5.1	0.820 ± 0.151	184.0 ± 2.1	19.4 ± 0.4	14.8 ± 0.2

In order to be simpler to analyse the effect of the weight content of reinforcement on the thermal properties of PVA, the variation of these properties is also presented in a graphic form-Figure 28.

a)

b)

c)

d)

e)
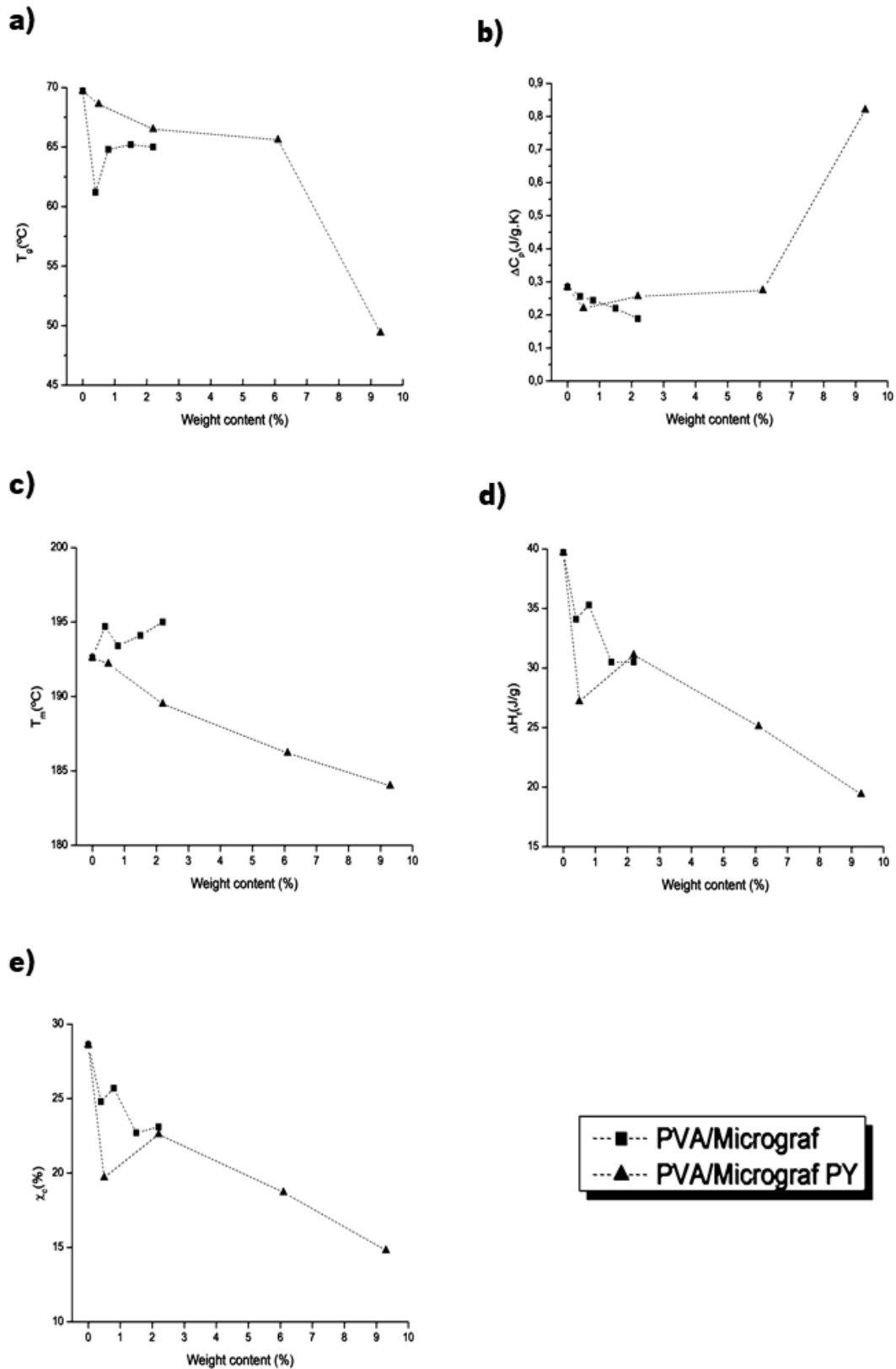
Figure 29: *a) Glass-transition temperature (T_g); b) heat capacity (ΔCp); c) melting temperature (T_m); d) enthalpy of fusion (ΔH_f); and e) cristalinity degree (χ_c) results as a function of the graphite weight content, obtained in first heating assays.*

As shown in Figure 29 a), the glass-transition temperature of PVA slightly decreases when Micrograf reinforcement increases from 0.4% to 2.2%. With the addition of exfoliated graphite, the glass

transition temperature of PVA decreases gradually from 69.7 °C to 49.4 °C when the filler content increases from 0.5% to 9.3%. Virtanen *et al.* reported a similar study for nanofibrillated cellulose, NFC/PVA composite films [130] and the reduction of T_g was attributed to the hydrogen bond barrier effect. So, the hydrogen bonds between PVA molecules are reduced when graphite or EG nanosheets are incorporated, increasing the mobility of the polymeric chains [131]. The heat capacity (Figure 29 b)) is 0.284 J/g·K for pure PVA and presents a significant increase for 9.3 wt% exfoliated graphite reaching a value of 0.820 J/g·K. For the other filler contents, the heat capacity remains approximately constant.

Figure 29 c) shows that there is no obvious change in the melting temperature of PVA in the composites reinforced with graphite, for the filler contents used. For EG, the melting temperature of pure PVA decreases with the increase of EG content from 192.6 °C to 184 °C at the highest EG content of 9.3 wt%. For PVA/Micrograf films the melting enthalpy presents a slight decrease, where for PVA/Micrograf PY films the decrease was higher (Figure 29 d)). The melting peak of PVA broadens and T_m decreases with the increase of EG content. The crystallinity degree (Figure 29 e)) decreases from 28.6% for pure PVA to 14.8% for PVA/Micrograf PY 9.3%. Probably, the hydrogen bonding interactions between graphite/exfoliated graphite and PVA chains would damage the ordered arrangement of PVA chains, thereby decreasing the melting temperature and the crystallinity degree of PVA. This feature is more evident for higher contents of filler. The decrease in the crystallinity degree could also be justified by the non-homogeneous dispersion of reinforcement particles and by the existence of agglomerates. Salavagione *et al.* reported the same decrease in Tm and Xc with the increase of the filler content for PVA/rGO composite films [132].

3.6. Raman Spectroscopy

Raman spectroscopy was utilized to detect the incorporation of graphite and exfoliated graphite along the PVA composite films. Figure 30 a) present the Raman spectra of Micrograf powder and PVA/Micrograf films and in Figure 30 b) EG powder and composite films reinforced with exfoliated graphite. All the spectra show the presence of the characteristic D, G, and 2D bands of carbon materials, that are absent in pure PVA films. The D band, near 1350 cm^{-1}, is related to the presence of structural defects in the hexagonal sp^2 carbon lattice of graphene. The G peak, near 1580 cm^{-1}, corresponds to the E_{2g} phonon at the Brillouin zone center that is related to the plane vibration of the sp^2 carbon atoms. The number of layers for graphene can be estimated by analysing the shape, width, and position of the 2D band, near 2700 cm^{-1} [133,134].

The analysis of the Raman spectra of Micrograf and Micrograf PY in Figure 30 a) and b), shows that the 2D band of exfoliated graphite is downshifted to a lower wavenumber which indicates that the exfoliation was successfully achieved. Around Raman shift of 2710 cm^{-1} and symmetric shape of the 2D band in Micrograf PY confirm the few-layer nature of the functionalized graphene obtained from graphite. The small peaks observed in Micrograf PY Raman spectra at approximately 1400 cm^{-1} and 1620 cm^{-1} are characteristic of the modified pyrene [135]. The Raman shift of PVA peak for PVA and composites was approximately 2900 cm^{-1}. The spectrum obtained of composites is a superposition of that of the graphite or EG and PVA. Thus, PVA does not affect the structure of the embedded flakes.
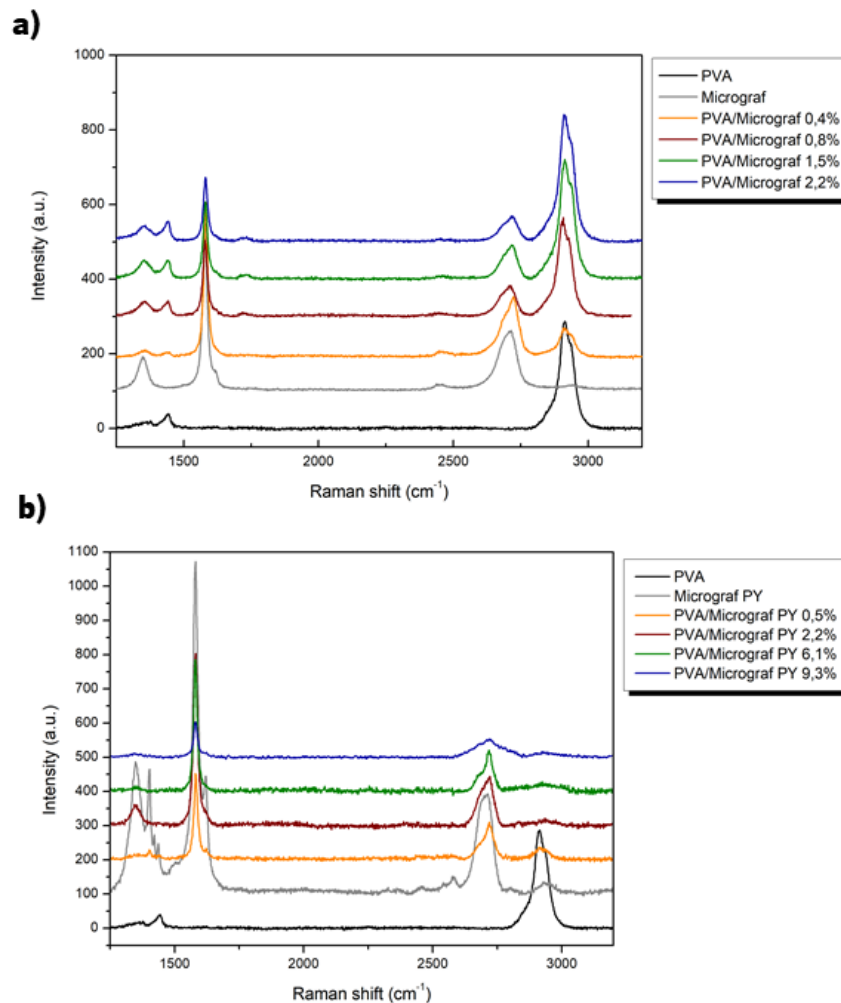
Figure 30: *Raman spectra of a) Micrograf and composite films reinforced with Micrograf; and b) Micrograf PY and composite films reinforced with Micrograf functionalyzed with pyrene*

3.7. Mechanical Characterization – Uniaxial Tensile tests

Uniaxial tensile tests were performed to analyse the effect of the incorporation of graphite and exfoliated graphite on the mechanical properties of PVA. The values obtained are showed in Table 7. The representative stress-strain curves of PVA and the respective composites are shown in Figure 31.
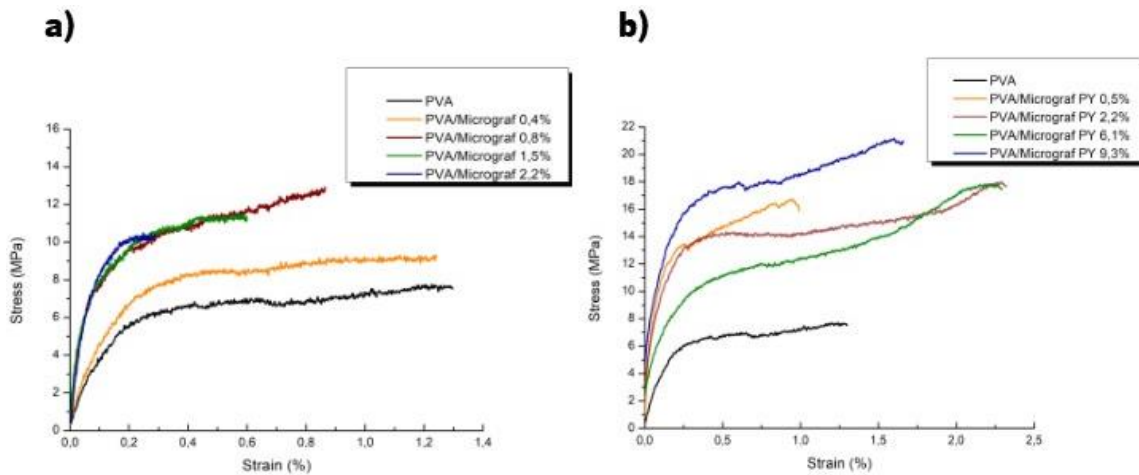
Figure 31: *Stress-strain curves for a) PVA/Micrograf; and b) PVA/Micrograf PY films subjected to uniaxial tensile tests.*

Figure 32 a), b), c) and d) present, respectively, the yield stress, the tensile strength, strain at break, and Young's modulus values obtained after the analysis of the stress-strain curves of Figure 31.
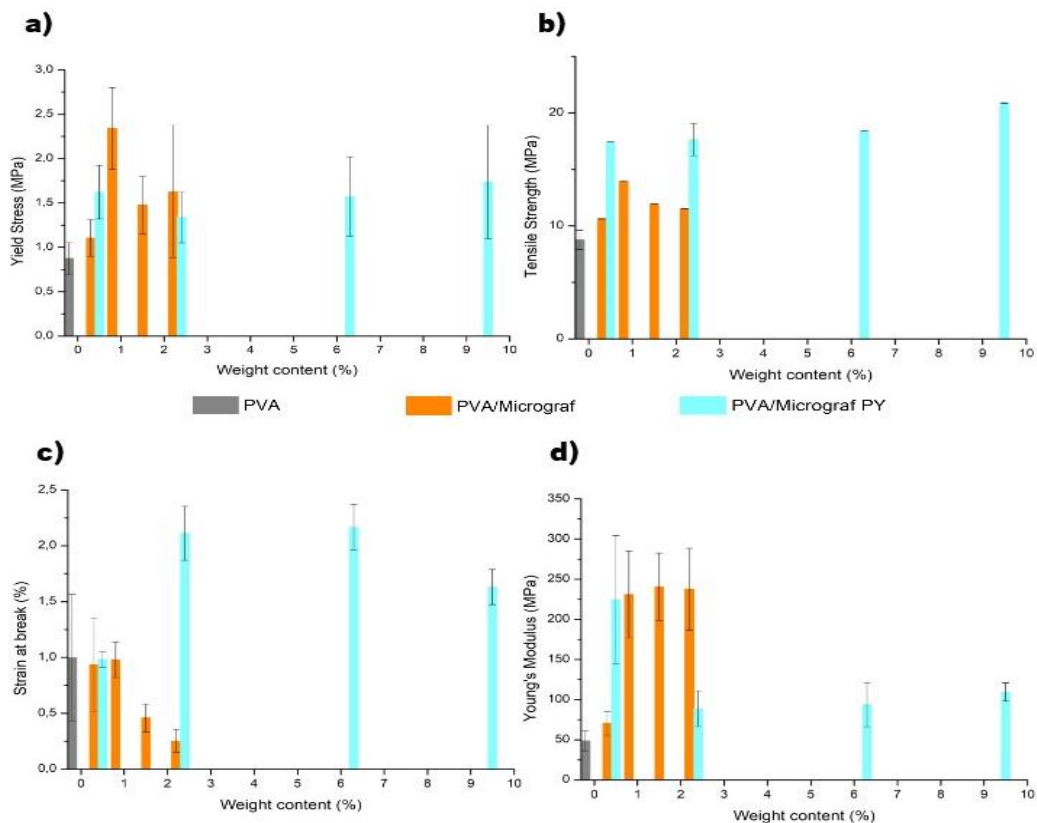
Figure 32: *a) yield stress; (b) tensile strength; c) strain at break; and d) Young's modulus of PVA, PVA/Micrograf and PVA/Micrograf PY composites.*

Chapter 3. Results and Discussion

As shown in Figure 32 a), a significant improvement in the yield stress was found for PVA/Micrograf 0.8%, raising from 0.88 MPa to 2.34 MPa. For the composite films reinforced with exfoliated graphite the increase was lower when compared with the films mentioned before, achieving a maximum of 1.74 MPa for 9.3 wt% EG. A simultaneous increase in the tensile strength and in the strain at break was observed with the incorporation of exfoliated graphite in the composite films, as shown in Figure 32 b) and c). The tensile strength raised from 8.77 MPa to 13.93 MPa for 0.8 wt% graphite and to 20.88 MPa for 9.3 wt% EG. This improvement is in agreement with the SEM results, that revealed an excellent interaction between PVA and graphite/exfoliated graphite. For PVA/Micrograf films, the strain at break decreased, from 0.99 % to 0.25 %, when the filler content was 2.2 wt%. The strain at break for the films reinforced with exfoliated graphite, raised from 0.99 % to 2.17%, when EG was 6.1 wt%. The Young's Modulus had a significant increase for composite films with graphite loadings higher than 0.8 wt% and for 0.5 wt% of exfoliated graphite, reaching a maximum value of 241 MPa for 1.5 wt% graphite (Figure 32 d). For exfoliated graphite loadings higher than 2.2 wt% the Young's Modulus decreased relatively to 0.5 wt%, but it is still higher than the PVA value (48.63 MPa). So, According to Wan *et al.*, such a large improvement in the mechanical properties of PVA composite films as the one seen in the present work could be attributed to the properties of the graphene derivative layers, the uniform dispersion of the graphene nanosheets throughout the polymer matrix, the aligned distribution of graphene derivatives parallel to the surface of the sample films and the strong hydrogen bonding interactions between the particles and polymer chains [136]. Also, the simultaneous improvement in the mechanical strength and ductility of polymer nanocomposites has been reported by Ma *et al.* with the incorporation of graphene oxide [137]. They also reported a decrease of Young's Modulus for GO loadings higher than 0.8 wt% [137].

It is necessary to mention that the strain at break is in the range of 164–219%, which can be taken as a small change in the elongation behaviour and is different from some previous works that have used graphene derivatives as reinforcing materials of PVA [114,138], in which the addition of graphene derivatives embrittled the PVA matrix and the elongation at break declines markedly. This occurred because the strong H-bonding interactions between the graphene derivatives surface and PVA matrix cause typical restriction in the movement of the polymer chains and decreased the elongation behaviour. This behaviour was found for PVA/Micrograf films. On the contrary, the decreased crystallinity of the matrix would lower the restriction of PVA polymer chains in nanocomposites and increase the elongation behaviour [137]. This is proved with the PVA/Micrograf PY films, which had a significant decrease in the

crystallinity degree, resulting in an increase of the strain at break. Comparing the films reinforced with approximately the same weight content of graphite and exfoliated graphite, it's possible to observe that PVA/Micrograf PY present a better mechanical resistance due to the homogeneity of films and the presence of a large quantity of small size particles with good interaction between the matrix and the reinforcement.

Table 7: Uniaxial tensile results obtained for PVA and PVA composites

	Weight content (wt%)	Yield Stress (MPa)	Yield Strain (%)	Tensile Strength (MPa)	Strain at break (%)	Young's Modulus (MPa)
PVA	-	0.88 ± 0.18	0.014 ± 0.015	8.77 ± 0.85	0.99 ± 0.57	48.63 ± 12.63
PVA/Micrograf	0.4	1.11 ± 0.21	0.011 ± 0.002	10.63 ± 0.01	0.94 ± 0.42	70.69 ± 14.68
	0.8	2.34 ± 0.46	0.010 ± 0.001	13.93 ± 0.01	0.98 ± 0.16	230.79 ± 54.23
	1.5	1.48 ± 0.33	0.007 ± 0.002	11.92 ± 0.01	0.46 ± 0.12	240.68 ± 41.91
	2.2	1.63 ± 0.75	0.008 ± 0.004	11.51 ± 0.01	0.25 ± 0.10	237.67 ± 50.89
PVA/Micrograf PY	0.5	1.62 ± 0.30	0.004 ± 0.002	17.43 ± 0.01	0.98 ± 0.07	224.59 ± 79.54
	2.2	1.34 ± 0.29	0.015 ± 0.003	17.65 ± 1.44	2.11 ± 0.24	88.62 ± 22.12
	6.1	1.57 ± 0.45	0.013 ± 0.005	18.41 ± 0.01	2.17 ± 0.20	93.74 ± 27.52
	9.3	1.74 ± 0.64	0.019 ± 0.004	20.88 ± 0.02	1.63 ± 0.16	109.36 ± 11.39

3.8. Electrical Conductivity measurements

The electrical conductivity measurements were performed to evaluate the influence of the reinforcement in PVA matrix and the effect of exfoliated graphite in electrical properties. The electrical properties of polymeric composites depend on the characteristics of dispersion, conductive pathways or even agglomerates of the incorporated reinforcing loads [139]. The electrical conductivity of PVA and PVA composite films was calculated by considering the current passing through the sample in the voltage range between -10.0 and 10.0 V. The conductivity as a function of the different weight contents incorporated in the composite films are presented in Figure 33 and Table 8.
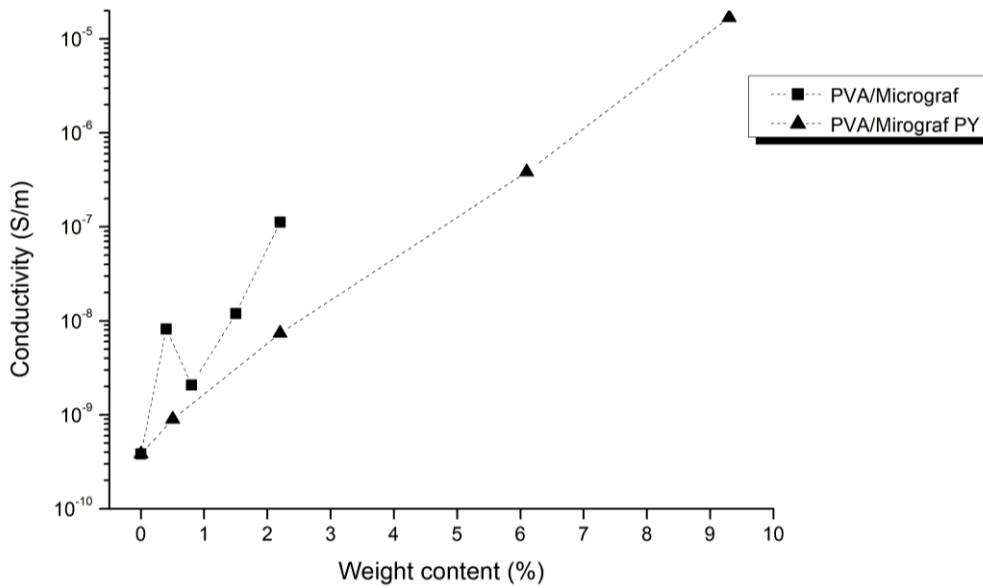
Figure 33: *Electrical conductivity measurements for PVA/Micrograf and PVA/Micrograf PY*

PVA films, as well as a large range of polymeric materials, has a behaviour like an electrical isolator material, with an electrical conductivity of 3.84×10^{-10} S/m. Figure 32 shows that when PVA is reinforced with weight contents superior of 1.5 wt%, the electrical conductivity has a significant increase. The incorporation of exfoliated graphite in the composite films resulted in an increase of the electrical conductivity from 3.84×10^{-10} S/m to 1.69×10^{-5} S/m for PVA/Micrograf PY 9.3 %. Mo *et al.* reported lower electrical conductivity for composite films containing graphene derivatives as fillers with 10 wt.% content [91]. The increase of the electrical conductivity observed in the present work could be attributed to the exfoliation of graphite that produces a large quantity of particles with small size, forming a conducting network in the PVA matrix. However, electrical percolation usually requires higher graphene derivative content.

By comparing PVA/Micrograf and PVA/Micrograf PY films (Figure 33), it can be seen that for the films reinforced with exfoliated graphite the electrical conductivity is much higher than for the films reinforced with graphite, which means that the exfoliation of graphite has a significant influence in the electrical properties of PVA composite films, increasing about 2 or 3 orders of magnitude for 6.1 wt% and 9.3 wt%. PVA/Micrograf PY 9.3% films present an electrical conductivity value typical of semiconductor materials. A similar conductivity study of PVA composite films reinforced with graphite and exfoliated graphite, produced by solvent casting was reported by S. Arantes [125]. The electrical properties obtained for PVA/Micrograf PY with weight content of 10% was 2.81×10^{-6} S/m, which is lower than PVA/Micrograf PY 9.3% value obtained in this work. So, it seems that the spray-drying method allows to produce films with higher electrical conductivity than those produced by solvent casting.

Table 8: *Resistivity and conductivity values obtained for electrical measurements of PVA and its composites*

	Weight content (wt%)	Resistivity ($\Omega \cdot m$)	Conductivity (S/m)
PVA	-	$2.77 \times 10^9 \pm 5.79 \times 10^8$	$3.84 \times 10^{-10} \pm 1.10 \times 10^{-10}$
PVA/Micrograf	0.4	$7.08 \times 10^8 \pm 7.32 \times 10^8$	$8.18 \times 10^{-9} \pm 9.40 \times 10^{-9}$
	0.8	$1.86 \times 10^9 \pm 1.30 \times 10^9$	$2.08 \times 10^{-9} \pm 2.98 \times 10^{-9}$
	1.5	$1.52 \times 10^8 \pm 9.19 \times 10^7$	$1.20 \times 10^{-8} \pm 9.55 \times 10^{-9}$
	2.2	$8.24 \times 10^7 \pm 9.91 \times 10^7$	$1.12 \times 10^{-7} \pm 9.96 \times 10^{-8}$
PVA/Micrograf PY	0.5	$1.38 \times 10^9 \pm 6.57 \times 10^8$	$9.00 \times 10^{-10} \pm 4.00 \times 10^{-10}$
	2.2	$2.76 \times 10^8 \pm 2.03 \times 10^8$	$7.38 \times 10^{-9} \pm 5.66 \times 10^{-9}$
	6.1	$9.17 \times 10^6 \pm 8.87 \times 10^6$	$3.84 \times 10^{-7} \pm 4.27 \times 10^{-7}$
	9.3	$6.68 \times 10^6 \pm 9.44 \times 10^6$	$1.69 \times 10^{-5} \pm 2.09 \times 10^{-5}$

CHAPTER 4.

CONCLUSIONS AND FUTURE WORK

4. CONCLUSIONS AND FUTURE WORK

4.1. Conclusions

In the present work, PVA and PVA composite films reinforced with graphite and exfoliated graphite were developed in order to take advantage of the interesting properties of both materials for biomedical applications. At first, the spray coating technique was investigated with the objective of produce films with good quality. Then, functionalized few-layer graphene suspensions were successfully synthetized from Micrograf through stabilizer-assisted liquid phase exfoliation technique, in order to produce composite films with 0.2, 1.1, 2.9 and 4.5 wt%. Composite films reinforced with 0.4, 0.9, 2.6 and 4.2 wt% of graphite were also produced. To evaluate the properties of films, various characterizations techniques were used.

By observing SEM images it's possible to conclude that the interface between PVA and Micrograf graphite, as well as exfoliated graphite is good and efficient. Electron microscopy also allowed to observe the graphite accumulation effect in one side of Micrograf films, since the evaporation process of water the graphite particles deposited by gravity. This observation demonstrates the heterogeneity of the PVA/Micrograf films and it justifies the slight increase of mechanical properties. PVA/Micrograf PY films shows a great homogeneity and a presence of small size particles due to the exfoliation process. Because of these characteristics the mechanical properties of PVA/Micrograf PY films present a significant increase. Raman spectroscopy revealed a presence of carbon materials in all composite films.

Regarding the thermal characterization, with the TGA analyses was possible to conclude that PVA/Micrograf films starts to degrade at a temperature of 275°C, so the presence of graphite o does not modify this temperature. But for films with exfoliated graphite the degradation temperature has a significant decrease, starting at 250°C. DSC assays revealed that for composite films reinforced with 2.2 wt% graphite and EG, there are no variation in thermal properties, being T_g and crystallinity degree approximately equal, so it's possible to conclude that the exfoliation of graphite does not modify the thermal properties of PVA. Comparing 0.4 wt% graphite and 0.5 wt% EG films, a slight increase in glass transition temperature and decrease in crystallinity degree was observed, it can be due to the non-homogeneous dispersion of reinforcement particles and by the existence of agglomerates.

With the water vapour transmission tests, it is concluded that there are no significant variations with the incorporation of graphite/exfoliated graphite, and its behaviour tends to be worse than PVA films when weight contents superior of 6.1% was incorporated. The results of mechanical characterization through uniaxial tensile tests showed that the tensile strength of 0.5 and 2.2 wt% of exfoliated graphite

presents a better mechanical resistance when compared to 0.4 and 2.2 wt% of graphite, so it's possible to conclude that there are strong hydrogen bonding interactions between the particles and polymer chains and the exfoliation of graphite has a good influence in mechanical properties of PVA. The enhancement of mechanical of PVA-based films depends on the dispersion and the alignment of graphene-derivative sheets in PVA matrix which is verified in SEM images of PVA/Micrograf PY films.

Through the analysis of electrical assays, electrical conductivity of PVA was increased with the addition of graphite and exfoliated graphite. PVA composite films reinforced with exfoliated graphite present a significant increase for weight contents of 6.1 and 9.3 wt%. The PVA/Micrograf PY 9.3% presents an electrical conductivity value close to the characteristics of a semiconductor material. This indicates that a reasonable amount of graphite sheets dispersed in PVA matrix provides composites with characteristics of electrical conductivity similar to semiconductor materials. With these results it's possible to conclude that, the exfoliation of graphite benefited the electrical properties.

In terms of biological behaviour of PVA and PVA composite films, it was observed that PVA is unstable when is in contact with aqueous environments because of their hydrophilic nature. To increase PVA stability, a novel crosslinking modification through naturally origin components, Genipin and Glycine, was founded.

This project allowed to verify that electrical and mechanical properties have a greater impact on the final properties of PVA/Micrograf PY 9.3% films. Thus, these composites present potential characteristics for biomedical applications as membranes for the regeneration of cardiac, muscles and bone tissues, in which electrical conduction and mechanical resistance properties are important.

4.2. Future work

To explore the potential of the PVA composite films reinforced with exfoliated graphite for applications in the biomedical field. The following topics are suggested as future work:

I. Optimization of the processing technique by changing the substrate in order to obtain a constant thickness of films and homogeneity through films surface. And controlling the atmosphere of the place where films were produced to clean the environment around the films and to control the temperature.

II. Producing composite films with a low toxic natural cross linker, like Genipin with the objective of increase the stability of PVA in aqueous environments. This modification possibly the evaluation of films in biological field.

III. Biocompatibility studies should be performed, depending on the intended application, increasing the diversity of potential applications.

REFERENCES

[1]   Y. Shin, S.-J. Song, S. Hong, S. Jeong, W. Chrzanowski, J.-C. Lee, D.-W. Han, Multifaceted biomedical applications of functional graphene nanomaterials to coated substrates, patterned arrays and hybrid scaffolds, Nanomaterials. 7 (2017) 369.

[2]   K. Nešović, M.M. Abudabbus, K.Y. Rhee, V. Mišković-Stanković, Graphene based composite hydrogel for biomedical applications, Croat. Chem. Acta. 90 (2017) 207–213.

[3]   E. Marin*, J. Rojas, Y. Ciro, A review of polyvinyl alcohol derivatives: Promising materials for pharmaceutical and biomedical applications, African J. Pharm. Pharmacol. 8 (2014) 674–684.

[4]   K.S. Novoselov, V.I. Fal'Ko, L. Colombo, P.R. Gellert, M.G. Schwab, K. Kim, A roadmap for graphene, Nature. 490 (2012) 192–200.

[5]   J. Kim, Applications of graphene and graphene-related materials, (2016) 1927–1945.

[6]   H. Stirring, C. Degassing, Graphite, graphene, and their polymer nanocomposites, (2013) 330–343.

[7]   H.O. Pierson, Handbook of carbon, graphite, diamond and fullerenes, Noyes Publications, Albuquerque, 1993.

[8]   M. Terrones, A.R. Botello-Méndez, J. Campos-Delgado, F. López-Urías, Y.I. Vega-Cantú, F.J. Rodríguez-Macías, A.L. Elías, E. Muñoz-Sandoval, A.G. Cano-Márquez, J.C. Charlier, H. Terrones, Graphene and graphite nanoribbons: Morphology, properties, synthesis, defects and applications, Nano Today. 5 (2010) 351–372.

[9]   C. Ho, C. Chang, M.-F. Lin, Landau subband wave functions and chirality manifestation in rhombohedral graphite, Solid State Commun. (2014) 1–14.

[10]   P. Mukhopadhyay, R. Gupta, Graphite, graphene, and their polymer nanocomposites, Taylor & Francis Group, London, 2013.

[11]   R. Sengupta, M. Bhattacharya, S. Bandyopadhyay, A.K. Bhowmick, A review on the mechanical and electrical properties of graphite and modified graphite reinforced polymer composites, Prog. Polym. Sci. 36 (2011) 638–670.

[12]   S. Picard, D.T. Burns, P. Roger, Determination of the specific heat capacity of a graphite sample using absolute and differential methods, Metrologia. 44 (2007) 294–302.

[13]   E. Falcao, F. Wudl, Carbon allotropes: beyond graphite and diamond, J. Chem. Technol. Biotechnol. 82 (2007) 524–531.

[14]   D.D.L. Chung, Review: Graphite, J. Mater. Sci. 37 (2002) 1475–1489.

[15]   S.A. Solin, The nature and structural properties of graphite intercalation compounds, Adv. Chem. Phys. 49 (1982) 455–532.

[16]   M.S. Dresselhaus, G. Dresselhaus, Advances in physics intercalation compounds of graphite, Adv. Phys. 51 (1981) 1–186.

[17]   D.D.L. Chung, Review: Exfoliation of graphite, J. Mater. Sci. 22 (1987) 4190–4198.

[18]   P.H. Chen, D.D.L. Chung, Thermal and electrical conduction in the compaction direction of exfoliated graphite and their relation to the structure, Carbon N. Y. 77 (2014) 538–550.

[19]   G.Z. Kyzas, E.A. Deliyanni, D.N. Bikiaris, A.C. Mitropoulos, Graphene composites as dye adsorbents: Review, Chem. Eng. Res. Des. 129 (2018) 75–88.

[20]   X. Li, W. Cai, J. An, S. Kim, J. Nah, D. Yang, R. Piner, A. Velamakanni, I. Jung, E. Tutuc, S.K. Banerjee, L. Colombo, R.S. Ruoff, Large area synthesis of high-quality and uniform graphene films on copper foils, Science (80-.). 324 (2009) 1312–1314.

[21]   G.Templeton,   What   is   graphene?,   ExtremeTech.   (2015). https://www.extremetech.com/extreme/211437-extremetech-explains-what-is-graphene.

[22]   Y. Yao, F. Ye, X.L. Qi, S.C. Zhang, Z. Fang, Spin-orbit gap of graphene: first-principles calculations, Phys. Rev. B - Condens. Matter Mater. Phys. 75 (2007) 2–5.

[23]   D.W. Boukhvalov, M.I. Katsnelson, A.I. Lichtenstein, Hydrogen on graphene: electronic structure, total energy, structural distortions and magnetism from first-principles calculations, Phys. Rev. B - Condens. Matter Mater. Phys. 77 (2008) 1–7.

[24]   M. Jaiswal, R. Menon, Polymer electronic materials: a review of charge transport, Polym. Int. 55 (2006) 1371–1384.

[25]   M. Allen, Honeycomb carbon – A study of graphene, Am. Chem. Soc. (2009) 184.

[26]   J.E.D. Vieira Segundo, E.O. Vilar, Grafeno: Uma revisão sobre propriedades, mecanismos de produção e potenciais aplicações em sistemas energéticos, Rev. Eletrônica Mater. E Process. 2 (2016) 54–57.

[27]   A.H.C. Neto, F. Guinea, N.M.R. Peres, K.S. Novoselov, A.K. Geim, The electronic properties of graphene, 81 (2007).

[28]   K.S. Divya, T.U. Umadevi, S. Mathew, Graphene-based semiconductor nanocomposites for photocatalytic applications, (2014) 1–34.

[29]   A.A. Balandin, S. Ghosh, W. Bao, I. Calizo, D. Teweldebrhan, F. Miao, C.N. Lau, Superior thermal

conductivity of single-layer graphene, Nano Lett. 8 (2008) 902–907.

[30] W. Cai, A.L. Moore, Y. Zhu, X. Li, S. Chen, L. Shi, R.S. Ruoff, Thermal transport in suspended and supported monolayer graphene grown by chemical vapor deposition, Nano Lett. 10 (2010) 1645–1651.

[31] C. Lee, X. Wei, J.W. Kysar, J. Hone, Measurement of the elastic properties and intrinsic strength of monolayer graphene, Science (80-.). 321 (2008) 385–388.

[32] J. Wang, F. Ma, W. Liang, M. Sun, Electrical properties and applications of graphene, hexagonal boron nitride (h-BN), and graphene/h-BN heterostructures, Mater. Today Phys. 2 (2017) 6–34.

[33] P. Avouris, Graphene: Electronic and photonic properties and devices, Nano Lett. 10 (2010) 4285–4294.

[34] Y. Zhu, S. Murali, W. Cai, X. Li, J.W. Suk, J.R. Potts, R.S. Ruoff, Graphene and graphene oxide: Synthesis, properties, and applications, Adv. Mater. 22 (2010) 3906–3924.

[35] P. Martin, Electrochemistry of gaphene: New horizons for sensing and energy storage, Chem. Rec. 9 (2009) 211–223.

[36] W.W. Liu, S.P. Chai, A.R. Mohamed, U. Hashim, Synthesis and characterization of graphene and carbon nanotubes: A review on the past and recent developments, J. Ind. Eng. Chem. 20 (2014) 1171–1185.

[37] O.C. Compton, S.T. Nguyen, Graphene oxide, highly reduced graphene oxide, and graphene: Versatile building blocks for carbon-based materials, Small. 6 (2010) 711–723.

[38] P.R. Somani, S.P. Somani, M. Umeno, Planer nano-graphenes from camphor by CVD, Chem. Phys. Lett. 430 (2006) 56–59.

[39] W. Choi, I. Lahiri, R. Seelaboyina, Y.S. Kang, Synthesis of graphene and its applications: A review, Crit. Rev. Solid State Mater. Sci. 35 (2010) 52–71.

[40] I. Forbeaux, J. Themlin, J. Debever, Heteroepitaxial graphite on Interface formation through conduction-band electronic structure, Phys. Rev. B - Condens. Matter Mater. Phys. 58 (1998) 16396–16406.

[41] C. Berger, Z. Song, T. Li, X. Li, A.Y. Ogbazghi, R. Feng, Z. Dai, A.N. Marchenkov, E.H. Conrad, P.N. First, W. Heer, Ultrathin epitaxial graphite, J. Phys. Chem. B. 108 (2004) 19912–19916.

[42] B.C. Brodie, On the atomic weight of graphite, Philos. Trans. R. Scociety London. 149 (1859) 249–259.

[43] L. Staudenmaier, Verfahren zur Darstellung der Graphitsaure, Berichte Der Dtsch. Chem.

Gesellschaft. 31 (1898) 1481–1487.

[44]   W.S. Hummers, R.E. Offeman, Preparation of graphitic oxide, J. Am. Chem. Soc. 80 (1958) 1339.

[45]   J. Zhang, H. Yang, G. Shen, P. Cheng, Reduction of graphene oxide via L-ascorbic acid, R. Soc. Chem. 46 (2010) 1112–1114.

[46]   Z. Fan, K. Wang, T. Wei, J. Yan, L. Song, B. Shao, An environmentally friendly and efficient route for the reduction of graphene oxide by aluminum powder, Carbon N. Y. 48 (2010) 1686–1689.

[47]   C. Zhu, S. Guo, Y. Fang, S. Dong, Reducing Sugar: New functional molecules for the green synthesis of graphene nanosheets, ACS Nano. 4 (2010) 2429–2437.

[48]   Y. Wang, Z. Shi, J. Yin, Facile synthesis of soluble graphene via a green reduction of graphene oxide in tea solution and its biocomposites, Am. Chem. Soc. 3 (2011) 1127–1133.

[49]   M. Zhang, R.R. Parajuli, D. Mastrogiovanni, B. Dai, P. Lo, W. Cheung, R. Brukh, P.L. Chiu, T. Zhou, Z. Liu, E. Garfunkel, H. He, Production of graphene sheets by direct dispersion with aromatic healing agents, Small. 6 (2010) 1100–1107.

[50]   A. Ciesielski, P. Samorì, Graphene via sonication assisted liquid-phase exfoliation, Chem. Soc. Rev. 43 (2014) 381–398.

[51]   S. Haar, M. El Gemayel, Y. Shin, G. Melinte, M.A. Squillaci, O. Ersen, C. Casiraghi, A. Ciesielski, P. Samorì, Enhancing the liquid-phase exfoliation of graphene in organic solvents upon addition of n-octylbenzene, Sci. Rep. 5 (2015) 1–9.

[52]   D. Parviz, S. Das, H.S.T. Ahmed, F. Irin, S. Bhattacharia, M.J. Green, Dispersions of non-covalently functionalized graphene with minimal stabilizer, ACS Nano. 6 (2012) 8857–8867.

[53]   Z. Chen, A. Lohr, C.R. Saha-Möller, F. Würthner, Self-assembled π-stacks of functional dyes in solution: structural and thermodynamic features, Chem. Soc. Rev. 38 (2009) 564–584.

[54]   L. Xu, J.W. McGraw, F. Gao, M. Grundy, Z. Ye, Z. Gu, J.L. Shepherd, Production of high-concentration graphene dispersions in low-boiling-point organic solvents by liquid-phase noncovalent exfoliation of graphite with a hyperbranched polyethylene and formation of graphene/ethylene copolymer composites, J. Phys. Chem. C. 117 (2013) 10730–10742.

[55]   T. Kuila, S. Bose, A.K. Mishra, P. Khanra, N.H. Kim, J.H. Lee, Chemical functionalization of graphene and its applications, Prog. Mater. Sci. 57 (2012) 1061–1105.

[56]   X. Ji, Y. Xu, W. Zhang, L. Cui, J. Liu, Review of functionalization, structure and properties of graphene/polymer composite fibers, Compos. Part A Appl. Sci. Manuf. 87 (2016) 29–45.

[57]   D. Li, M.B. Müller, S. Gilje, R.B. Kaner, G.G. Wallace, Processable aqueous dispersions of

graphene nanosheets, Nat. Nanotechnol. 3 (2008) 101–105.

[58]   V. Georgakilas, J.N. Tiwari, K.C. Kemp, J.A. Perman, A.B. Bourlinos, K.S. Kim, R. Zboril, Noncovalent functionalization of graphene and graphene oxide for energy materials, biosensing, catalytic, and biomedical applications, Chem. Rev. 116 (2016) 5464–5519.

[59]   V. Georgakilas, M. Otyepka, A.B. Bourlinos, V. Chandra, N. Kim, K.C. Kemp, P. Hobza, R. Zboril, K.S. Kim, Functionalization of graphene : covalent and non- covalent approaches , derivatives and applications, Chem. Rev. 112 (2012) 6156–6214.

[60]   J. Liu, J. Tang, J.J. Gooding, Strategies for chemical modification of graphene and applications of chemically modified graphene, J. Mater. Chem. 22 (2012) 12435.

[61]   M. Silva, N.M. Alves, M.C. Paiva, Graphene-polymer nanocomposites for biomedical applications, Polym. Adv. Technol. 29 (2018) 687–700.

[62]   M. Avella, M. Cocca, M.E. Errico, G. Gentile, Biodegradable PVOH-based foams for packaging applications, J. Cell. Plast. 47 (2011) 271–281.

[63]   K.Y. Lee, D.J. Mooney, Hydrogels for tissue engineering, Chem. Rev. 101 (2001) 1869–1879.

[64]   T. Miyata, T. Uragami, K. Nakamae, Biomolecule-sensitive hydrogels, Adv. Drug Deliv. Rev. 54 (2002) 79–98.

[65]   C.M. Hassan, N.A. Peppas, Structure and applications of poly(vinyl alcohol) hydrogels produced by conventional crosslinking or by freezing/thawing methods. Nanocomposites. 153 (2000) 37–65.

[66]   F.Y. Jiang, Poly (vinyl alcohol) for biomedical applications, 2009.

[67]   A. Kumar, S.S. Han, PVA-based hydrogels for tissue engineering: A review, Int. J. Polym. Mater. Polym. Biomater. 66 (2017) 159–182.

[68]   Y. Liu, L.M. Geever, J.E. Kennedy, C.L. Higginbotham, P.A. Cahill, G.B. McGuinness, Thermal behavior and mechanical properties of physically crosslinked PVA/Gelatin hydrogels, J. Mech. Behav. Biomed. Mater. 3 (2010) 203–209.

[69]   C.E. Schildknecht, Polyvinyl alcohol, properties and applications, J. Polym. Sci. Polym. Lett. Ed. 12 (1974) 105–106.

[70]   W. Sun, L. Chen, J. Wang, Degradation of PVA (polyvinyl alcohol) in wastewater by advanced oxidation processes, J. Adv. Oxid. Technol. 20 (2017).

[71]   E. Chiellini, A. Corti, S. D'Antone, R. Solaro, Biodegradation of poly (vinyl alcohol) based materials, 2003.

[72] T. Mori, M. Sakimoto, T. Kagi, T. Sakai, Isolation and Characterization of a Strain of Bacillus megaterium That Degrades Poly(vinyl alcohol), Biosci. Biotechnol. Biochem. 60 (1996) 330–332.

[73] R. Chandra, R. Rustgi, Biodegradable Polymers, Prog. Polym. Sci. 23 (1998) 1273–1335.

[74] S. Matsumura, N. Tomizawa, A. Toki, K. Nishikawa, K. Toshima, Novel Poly(vinyl alcohol)-Degrading Enzyme and the Degradation Mechanism, Macromolecules. 32 (1999) 7753–7761.

[75] J.A. Lee, M.N. Kim, Isolation of new and potent poly(vinyl alcohol)-degrading strains and their degradation activity, Polym. Degrad. Stab. 81 (2003) 303–308.

[76] E. Chiellini, A. Corti, G. Del Sarto, S. D'Antone, Oxo-biodegradable polymers - Effect of hydrolysis degree on biodegradation behaviour of poly(vinyl alcohol), Polym. Degrad. Stab. 91 (2006) 3397–3406.

[77] C.. C. DeMerlis, D.. R. Schoneker, Review of the oral toxicity of polyvinyl alcohol (PVA)., Food Chem. Toxicol. 41 (2003) 319–26.

[78] N. Limpan, T. Prodpran, S. Benjakul, S. Prasarpran, Influences of degree of hydrolysis and molecular weight of poly(vinyl alcohol) (PVA) on properties of fish myofibrillar protein/PVA blend films, Food Hydrocoll. 29 (2012) 226–233.

[79] T.M.C. Maria, R.A. de Carvalho, P.J.A. Sobral, A.M.B.Q. Habitante, J. Solorza-Feria, The effect of the degree of hydrolysis of the PVA and the plasticizer concentration on the color, opacity, and thermal and mechanical properties of films based on PVA and gelatin blends, J. Food Eng. 87 (2008) 191–199.

[80] E. De Souza Costa, M.M. Pereira, H.S. Mansur, Properties and biocompatibility of chitosan films modified by blending with PVA and chemically crosslinked, J. Mater. Sci. Mater. Med. 20 (2009) 553–561.

[81] M. Mahmoudi, A. Simchi, A.S. Milani, P. Stroeve, Cell toxicity of superparamagnetic iron oxide nanoparticles, J. Colloid Interface Sci. 336 (2009) 510–518.

[82] J.M. Yang, W.Y. Su, T.L. Leu, M.C. Yang, Evaluation of chitosan/PVA blended hydrogel membranes, J. Memb. Sci. 236 (2004) 39–51.

[83] M. Wang, Y. Li, J. Wu, F. Xu, Y. Zuo, J.A. Jansen, In vitro and in vivo study to the biocompatibility and biodegradation of hydroxyapatite / poly (vinyl alcohol)/ gelatin composite, Wiley Intersci. (2007).

[84] M. Kobayashi, Y. Chang, M. Oka, A two year in vivo study of polyvinyl alcohol-hydrogel (PVA-H) artificial meniscus, 26 (2005) 3243–3248.

[85]   S. Kaity, J. Isaac, A. Ghosh, Interpenetrating polymer network of locust bean gum-poly (vinyl alcohol) for controlled release drug delivery, Carbohydr. Polym. 94 (2013) 456–467.

[86]   C. Guo, L. Zhou, J. Lv, Effects of expandable graphite and modified ammonium polyphosphate on the flame-retardant and mechanical properties of wood flour-polypropylene composites, Polym. Polym. Compos. 21 (2013) 449–456.

[87]   C. Shuai, Z. Mao, H. Lu, Y. Nie, H. Hu, S. Peng, Fabrication of porous polyvinyl alcohol scaffold for bone tissue engineering via selective laser sintering, Biofabrication. 5 (2013).

[88]   V.H. Pham, T.V. Cuong, S.H. Hur, E.W. Shin, J.S. Kim, J.S. Chung, E.J. Kim, Fast and simple fabrication of a large transparent chemically-converted graphene film by spray-coating, Carbon N. Y. 48 (2010) 1945–1951.

[89]   Y. Liu, D. Zhang, Synergetic effect in the multifunctional composite film of graphene-TiO2with transparent conductive, photocatalytic and strain sensing properties, J. Alloys Compd. 698 (2017) 60–67.

[90]   A.N. Sprafke, D. Schneevoigt, S. Seidel, S.L. Schweizer, R.B. Wehrspohn, Automated spray coating process for the fabrication of large-area artificial opals on textured substrates, Opt. Express. 21 (2013) A528–A538.

[91]   C. Girotto, B.P. Rand, J. Genoe, P. Heremans, Exploring spray coating as a deposition technique for the fabrication of solution-processed solar cells, Sol. Energy Mater. Sol. Cells. 93 (2009) 454–458.

[92]   Indriyati, R. Yudianti, M. Karina, Development of nanocomposites from bacterial cellulose and poly(vinyl Alcohol) using casting-drying method, Procedia Chem. 4 (2012) 73–79.

[93]   J.S. Gonzalez, L.N. Ludueña, A. Ponce, V.A. Alvarez, Poly(vinyl alcohol)/cellulose nanowhiskers nanocomposite hydrogels for potential wound dressings, Mater. Sci. Eng. C. 34 (2014) 54–61.

[94]   Y. Shi, D. Xiong, J. Zhang, Effect of irradiation dose on mechanical and biotribological properties of PVA/PVP hydrogels as articular cartilage, Tribol. Int. 78 (2014) 60–67.

[95]   S. Bonakdar, S.H. Emami, M.A. Shokrgozar, A. Farhadi, S.A.H. Ahmadi, A. Amanzadeh, Preparation and characterization of polyvinyl alcohol hydrogels crosslinked by biodegradable polyurethane for tissue engineering of cartilage, Mater. Sci. Eng. C. 30 (2010) 636–643.

[96]   S. Mo, L. Peng, C. Yuan, C. Zhao, W. Tang, C. Ma, J. Shen, W. Yang, Y. Yu, Y. Min, A.J. Epstein, Enhanced properties of poly(vinyl alcohol) composite films with functionalized graphene, RSC Adv. 5 (2015) 97738–97745.

[97] J. Liang, Y. Huang, L. Zhang, Y. Wang, Y. Ma, T. Cuo, Y. Chen, Molecular-level dispersion of graphene into poly(vinyl alcohol) and effective reinforcement of their nanocomposites, Adv. Funct. Mater. 19 (2009) 2297–2302.

[98] D. Liu, Q. Bian, Y. Li, Y. Wang, A. Xiang, H. Tian, Effect of oxidation degrees of graphene oxide on the structure and properties of poly (vinyl alcohol) composite films, Compos. Sci. Technol. 129 (2016) 146–152.

[99] H. Liu, P. Bandyopadhyay, N.H. Kim, B. Moon, J.H. Lee, Surface modified graphene oxide/poly(vinyl alcohol) composite for enhanced hydrogen gas barrier film, Polym. Test. 50 (2016) 49–56.

[100] N. Theophile, H.K. Jeong, Electrochemical properties of poly(vinyl alcohol) and graphene oxide composite for supercapacitor applications, Chem. Phys. Lett. 669 (2017) 125–129.

[101] W. Liu, H. Zhao, Y. Inoue, X. Wang, P.D. Bradford, H. Kim, Y. Qiu, Y. Zhu, Poly(vinyl alcohol) reinforced with large-diameter carbon nanotubes via spray winding, Compos. Part A Appl. Sci. Manuf. 43 (2012) 587–592.

[102] Y. Chen, L. Zhang, H. Zhan, J.N. Wang, New processing method to fabricate high-performance carbon-nanotube/polyvinyl alcohol composite films, Carbon N. Y. 110 (2016) 490–496.

[103] C. Yu, B. Li, Morphology and properties of conducting polyvinyl alcohol hydrosulfate/graphite nanosheet composites, J. Compos. Mater. 42 (2008) 1491–1504.

[104] H. Bin Zhang, W.G. Zheng, Q. Yan, Y. Yang, J.W. Wang, Z.H. Lu, G.Y. Ji, Z.Z. Yu, Electrically conductive polyethylene terephthalate/graphene nanocomposites prepared by melt compounding, Polymer (Guildf). 51 (2010) 1191–1196.

[105] S. Vadukumpully, J. Paul, N. Mahanta, S. Valiyaveettil, Flexible conductive graphene/poly(vinyl chloride) composite thin films with high mechanical strength and thermal stability, Carbon N. Y. 49 (2011) 198–205.

[106] X.S. Du, M. Xiao, Y.Z. Meng, Facile synthesis of highly conductive polyaniline/graphite nanocomposites, Eur. Polym. J. 40 (2004) 1489–1493.

[107] Q. Wu, Y. Xu, Z. Yao, A. Liu, G. Shi, Supercapacitors based on flexible graphene/polyaniline nanofiber composite films, ACS Nano. 4 (2010) 1963–1970.

[108] H. Kim, C.W. Macosko, Processing-property relationships of polycarbonate/graphene composites, Polymer (Guildf). 50 (2009) 3797–3809.

[109] M. Zahid, E.L. Papadopoulou, A. Athanassiou, I.S. Bayer, Strain-responsive mercerized conductive

cotton fabrics based on PEDOT:PSS/graphene, Mater. Des. 135 (2017) 213–222.

[110] Q. Chen, F. Zabihi, M. Eslamian, Improved functionality of PEDOT:PSS thin films via graphene doping, fabricated by ultrasonic substrate vibration-assisted spray coating, Synth. Met. 222 (2016) 309–317.

[111] S. Watcharotone, D. a Dikin, S. Stankovich, R. Piner, I. Jung, G.H.B. Dommett, G. Evmenenko, S.E. Wu, S.F. Chen, C.P. Liu, S.T. Nguyen, Graphene- Silica Composite Thin Films as Transparent Conductors, Nano Lett. 7 (2007) 1888–1892.

[112] W. Zheng, S.C. Wong, Electrical conductivity and dielectric properties of PMMA/expanded graphite composites, Compos. Sci. Technol. 63 (2003) 225–235.

[113] D. Han, L. Yan, W. Chen, W. Li, Preparation of chitosan/graphene oxide composite film with enhanced mechanical strength in the wet state, Carbohydr. Polym. 83 (2011) 653–658.

[114] L. Zhang, Z. Wang, C. Xu, Y. Li, J. Gao, Y. Liu, High strength graphene oxide/polyvinyl alcohol composite hydrogels, J. Mater. Chem. 21 (2011) 10399–10406.

[115] H. Huang, P. Ren, J. Chen, W. Zhang, X. Ji, Z. Li, High barrier graphene oxide nanosheet / poly (vinyl alcohol) nanocomposite films, 410 (2012) 156–163.

[116] W. Liu, X. Zhang, G. Xu, P.D. Bradford, X. Wang, H. Zhao, Y. Zhang, Q. Jia, F.G. Yuan, Q. Li, Y. Qiu, Y. Zhu, Producing superior composites by winding carbon nanotubes onto a mandrel under a poly(vinyl alcohol) spray, Carbon N. Y. 49 (2011) 4786–4791.

[117] H. Yang, L. Pan, Y. Han, L. Ma, Y. Li, H. Xu, J. Zhao, A visual water vapor photonic crystal sensor with PVA/SiO 2 opal structure, Appl. Surf. Sci. 423 (2017) 421–425.

[118] J. Huang, S. Lyu, F. Fu, Y. Wu, S. Wang, Green preparation of a cellulose nanocrystals/polyvinyl alcohol composite superhydrophobic coating, RSC Adv. 7 (2017) 20152–20159.

[119] X. Zhao, Q. Zhang, D. Chen, P. Lu, Enhanced mechanical properties of graphene-based polyvinyl alcohol composites, Macromolecules. 43 (2010) 2357–2363.

[120] L. Wang, W. Wang, P. Fan, M. Zhou, J. Yang, F. Chen, Ionic liquid modified graphene / poly (vinyl alcohol) composite with enhanced properties, Appl. Polym. Sci. 45006 (2017) 1–10.

[121] R. Balint, S.H. Cartmell, Electrical Stimulation : A Novel Tool, 19 (2013) 48–57.

[122] T.H. Qazi, R. Rai, A.R. Boccaccini, Tissue engineering of electrically responsive tissues using polyaniline based polymers : A review, Biomaterials. (2014) 1–19.

[123] G.S. Bumbrah, R.M. Sharma, Raman spectroscopy – Basic principle , instrumentation and selected applications for the characterization of drugs of abuse, Egypt. J. Forensic Sci. (2015).

[124] E. Freire, Differential Scanning Calorimetry, in: S. B.A. (Ed.), Protein Stab. Folding. Methods Mol. Biol., Humana Press, New Jersey, 1995: pp. 191–218.

[125] G. Michler, Electron Microscopy of Polymers, Springer Science & Business Media, 20AD.

[126] R.F. Egerton, Physical principles of electron microscopy, Springer US, Boston, 2005.

[127] D. Carrol, Introduction to Tensile Testing, in: Tensile Test., Second Edi, ASM International, 2004: p. 283.

[128] B. Tissue, Ultraviolet and visible absorption spectroscopy, in: Charact. Mater., 1st ed., Virginia, 2002: pp. 688–698.

[129] H.-H. Perkampus, UV-Vis Spectroscopy and its Aplications, Springer-Verlag, Berlin, 2002.

[130] S. Arantes, Filmes baseados em PVA e Grafeno para Aplicações Biomédicas, Universidade do Minho, 2018.

[131] Y. Liu, D. Zhang, The preparation of reduced graphene oxide-TiO2composite materials towards transparent, strain sensing and photodegradation multifunctional films, Compos. Sci. Technol. 137 (2016) 102–108.

[132] Y. Xu, W. Hong, H. Bai, C. Li, G. Shi, Strong and ductile poly(vinyl alcohol)/graphene oxide composite films with a layered structure, Carbon N. Y. 47 (2009) 3538–3543.

[133] M. Galotto, P. Ulloa, Effect of high-pressure food processing on the mass transfer properties of selected packaging materials, Packag. Technol. Sci. 23 (2010) 253–266.

[134] Y. Cao, W. Wei, J. Liu, Q. You, F. Liu, Q. Lan, C. Zhang, C. Liu, J. Zhao, The Preparation of Graphene Reinforced Poly (vinyl alcohol) Antibacterial Nanocomposite Thin Film, 2015 (2015) 1–21.

[135] S. Virtanen, J. Vartianen, H. Setälä, T. Tammelin, S. Vuoti, Modified nanofibrillated cellulose-polyvinyl alcohol films with improved mechanical performance, RSC Adv. 4 (2014) 11343–11350.

[136] C. Bao, Y. Guo, L. Song, Y. Hu, Poly(vinyl alcohol) nanocomposites based on graphene and graphite oxide: A comparative investigation of property and mechanism, J. Mater. Chem. 21 (2011) 13942–13950.

[137] H.J. Salavagione, G. Martínez, M.A. Gómez, Synthesis of poly(vinyl alcohol)/reduced graphite oxide nanocomposites with improved thermal and electrical properties, J. Mater. Chem. 19 (2009) 5027–5032.

[138] A.C. Ferrari, Raman spectroscopy of graphene and graphite: Disorder, electron-phonon coupling, doping and nonadiabatic effects, Solid State Commun. 143 (2007) 47–57.

[139] A.C. Ferrari, D.M. Basko, Raman spectroscopy as a versatile tool for studying the properties of graphene, Nat. Nanotechnol. 8 (2013) 235–246.

[140] H. Shinohara, Y. Yamakita, K. Ohno, Raman spectra of polycyclic aromatic hydrocarbons. Comparison of calculated raman intensity distributions with observed spectra for naphthalene, anthracene, pyrene, and perylene, J. Mol. Struct. 442 (1998) 221–234.

[141] C. Wan, B. Chen, Reinforcement and interphase of polymer/graphene oxide nanocomposites, J. Mater. Chem. 22 (2012) 3637–3646.

[142] J. Ma, Y. Li, X. Yin, Y. Xu, J. Yue, J. Bao, T. Zhou, Poly(vinyl alcohol)/graphene oxide nanocomposites prepared by in situ polymerization with enhanced mechanical properties and water vapor barrier properties, RSC Adv. 6 (2016) 49448–49458.

[143] X. Yang, L. Li, S. Shang, X. ming Tao, Synthesis and characterization of layer-aligned poly(vinyl alcohol)/graphene nanocomposites, Polymer (Guildf). 51 (2010) 3431–3435.

[144] K.K. Sadasivuni, D. Ponnamma, J. Kim, S. Thomas, Graphene-based polymer nanocomposites in electronics, Graphene-Based Polym. Nanocomposites Electron. (2015) 1–382.

[145] Sanaz Alhosseini, F. Moztarzadeh, A. Karkhaneh, Genipin-crosslinked Polyvinyl Alcohol for Neural Scaffold, Tehran, 2017.
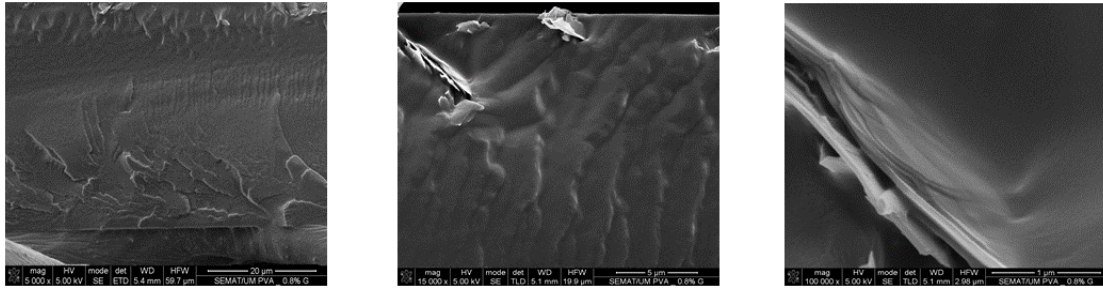
ANEXO I – SCANNING ELECTRON MICROSCOPY

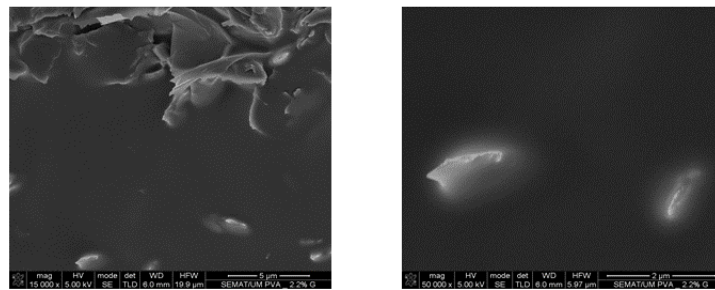**Figure 34:** *SEM images of PVA/Micrograf 0.8%*

Figure 35: *SEM images of PVA/Micrograf 2.2%*
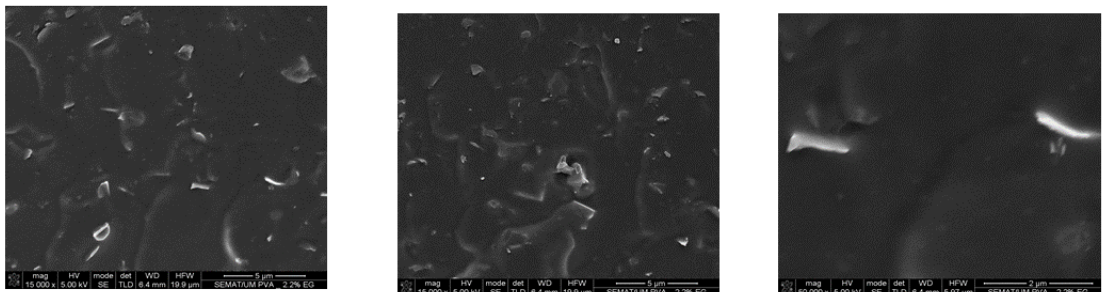

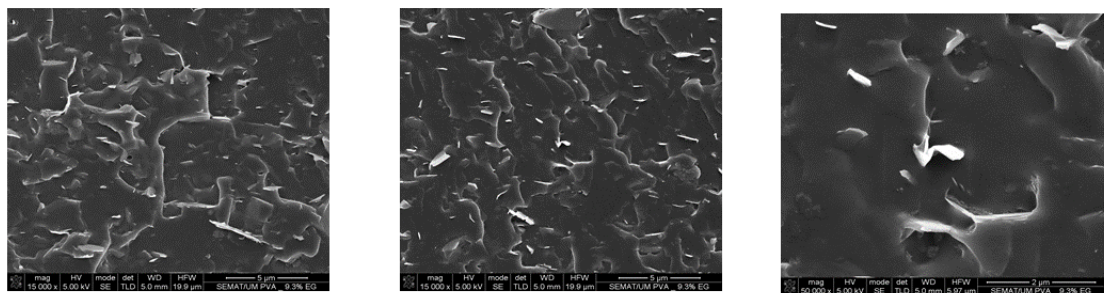**Figure 36:** *SEM images of PVA/Micrograf PY 2.2 %*

Figure 37: *SEM images of PVA/Micrograf PY 9.3%*

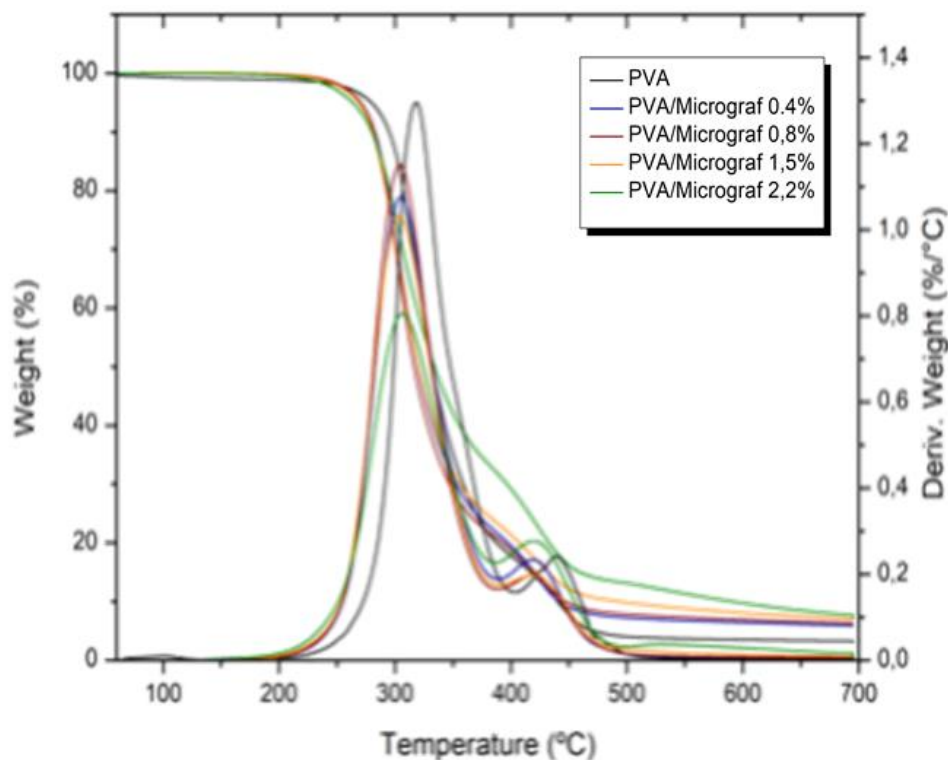# ANEXO II – THERMOGRAVIMETRIC ANALYSIS RESULTS

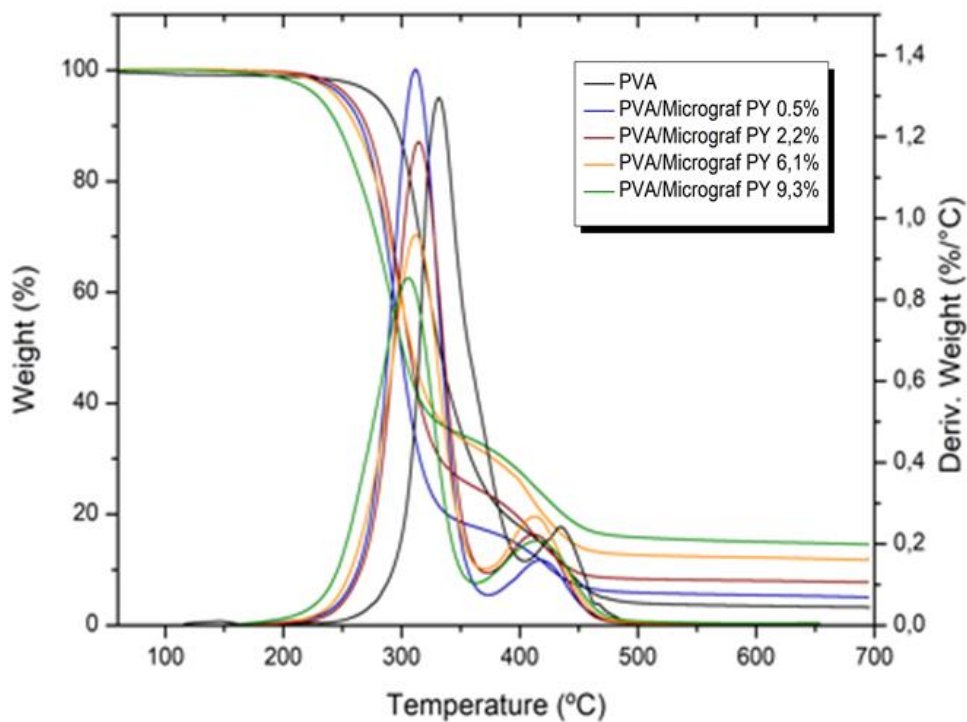**Figure 38:** *TGA curves for PVA/Micrograf from zone B of films*

Figure 39: *TGA curves for PVA/Micrograf PY from zone B of films*